ACS SyntheticBiology

pubs.acs.org/synthbio Research Article

Naked Bacterium: Emerging Properties of a Surfome-Streamlined *Pseudomonas putida* Strain

Esteban Martínez-García, Sofía Fraile, David Rodríguez Espeso, Davide Vecchietti, Giovanni Bertoni, and Víctor de Lorenzo*

Cite This: *ACS Synth. Biol.* 2020, 9, 2477–2492 Read Online

ACCESS | Metrics & More | Article Recommendations | Supporting Information

ABSTRACT: Environmental bacteria are most often endowed with native surface-attachment programs that frequently conflict with efforts to engineer biofilms and synthetic communities with given tridimensional architectures. In this work, we report the editing of the genome of *Pseudomonas putida* KT2440 for stripping the cells of most outer-facing structures of the bacterial envelope that mediate motion, binding to surfaces, and biofilm formation. To this end, 23 segments of the *P. putida* chromosome encoding a suite of such functions were deleted, resulting in the surface-naked strain EM371, the physical properties of which changed dramatically in respect to the wild type counterpart. As a consequence, surface-edited *P. putida* cells were unable to form biofilms on solid supports and, because of the swimming deficiency and other alterations, showed a much faster sedimentation in liquid media. Surface-naked bacteria were then used as carriers of interacting partners (e.g., Jun−Fos domains) ectopically expressed by means of an autotransporter display system on the now easily accessible cell envelope. Abstraction of individual bacteria as adhesin-coated spherocylinders enabled rigorous quantitative description of the multicell interplay brought about by thereby engineered physical interactions. The model was then applied to parametrize the data extracted from automated analysis of confocal microscopy images of the experimentally assembled bacterial flocks for analyzing their structure and distribution. The resulting data not only corroborated the value of *P. putida* EM371 over the parental strain as a platform for display artificial adhesins but also provided a strategy for rational engineering of catalytic communities.

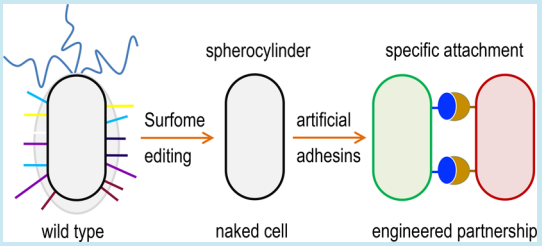

KEYWORDS: *Pseudomonas putida, genome reduction, surface display, artificial adhesins, bacterial adhesion*

Although the fundamental and biotechnological value of engineering microbial communities is beyond any doubt,[1−3] the endeavor is often limited by the fact that naturally occurring bacteria have their own surface-attachment agenda.[4−6] This makes native adhesion properties and endogenous biofilm formation programs to interfere with efforts to engineer multistrain interactions and/or programmable biofilms. The logical way forward is suppression of the innate mechanisms of surface adhesion and replacement by artificial counterparts. Because many types of bacteria control a switch between sessile and surface-attached lifestyles by regulating the intracellular levels of cyclic-di-GMP,[7−9] it comes as little surprise that most efforts thus far to manage adhesion have attempted to override the endogenous cyclic-di-GMP regulon, *e.g.*, by heterologous expression of a specific cyclase.[10] An alternative approach involves the display of heterologous adhesins on the bacterial surface, typically protein interacting partners thereof[11] or nanobodies/matching antigens,[12−14] so that their conditional expression brings about more or less structured multicell assemblies. While this last strategy looks more promising for engineering bacterial communities with given tridimensional (3D) structures, it relies on mutual accessibility of the interacting partners that protrude from the outer cell membrane. This is often made difficult by the presence of a suite of envelope components that impede direct contact between bacterial surfaces. The envelope of Gram-negative bacteria is characteristically composed of an inner membrane, a peptidoglycan layer, and an asymmetrical outer membrane (OM) that is directly facing the environment. The OM is composed of polyanionic lipopolysaccharides and phospholipids in outer and inner layers which in turn hold lipoproteins, porins, gated-channels and exports systems.[15,16] Yet, the OM is also the scaffold of a suite of nonlipidic structures on its outward-facing layer that allows interactions with the environment in different ways, *e.g.*, swimming to explore different niches (flagella), intercell adhesion, or attachment to solid surfaces (pili, fimbriae, surface proteins and exopolysaccharides;[6,17]). While these structures are important for enduring different environmental challenges,

Received: May 19, 2020
Published: July 30, 2020

https://dx.doi.org/10.1021/acssynbio.0c00272
ACS Synth. Biol. 2020, 9, 2477−2492

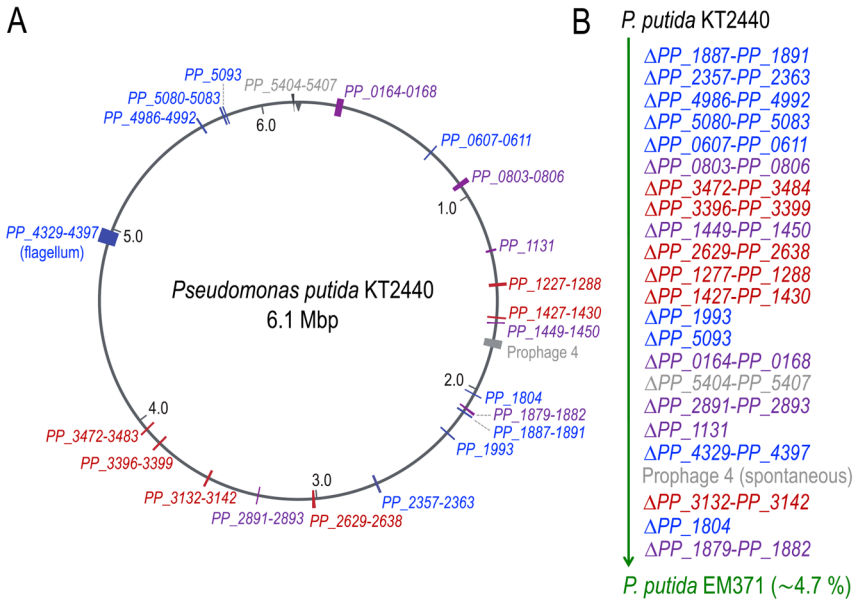

Figure 1. Construction of surfome-streamlined strain *P. putida* EM371. (A) genetic map of *P. putida* KT2440 depicting the approximate location of the operons deleted to engineer the surface display strain. Not drawn to scale. (B) Pipeline followed to engineer *P. putida* EM371 strain. The serial deletion steps with the relevant PP numbers of the regions or genes deleted are depicted in the proper order. These deletions resulted in a *P. putida* variant with a 4.7% genome reduction. The different colors in the figure represent the artificial clustering of these regions. In blue are represented regions within the complex structures group. In purple are surface proteins. In dark red are the EPS-related ones. In gray are the other elements.

they may be otherwise dispensable for biotechnological applications[18,19] including the above-mentioned design of structured bacterial consortia.[20]

In order to expand the utilities of *Pseudomonas putida* as a prime synthetic biology chassis for industrial and environmental uses, we set out to edit the genome of the reference strain KT2440 to make it an optimal biological frame for surface display of artificial adhesins. *P. putida* KT2440 is a nonpathogenic, HV1 certified,[21] soil inhabitant and root colonizer endowed with a robust metabolism. Its diverse biochemical capacities enable this strain to use a broad number of substrates as carbon sources and to host strong redox reactions.[22−24] Moreover, it is highly resistant to organic solvents,[25] and it is amenable to a large number of genetic manipulations.[26−28] Taken together, these properties make *P. putida* KT2440 a platform of choice for bioproduction of value-added compounds.[29−31] Alas, as is the case with other *Pseudomonas*, *P. putida* KT2440 also has a complex cell envelope with a number of structures that obstruct the access to proteins closely attached to the cell surface or artificially designed adhesins thereof.

In this work, we have scanned the genome of *P. putida* KT2440 to identify nonessential genes encoding surface-protruding structures innately exposed on the OM. Most of them were serially deleted to generate cells with a less complex and more accessible outer cell surface. This operation resulted in an envelope-streamlined strain that was morphologically and phenotypically characterized and also tested as the carrier of artificial adhesins displayed on the cell envelope by means of genetically encoded autotransporter domains.[11,32] The data below not only demonstrate that removing surface structures improve, very significantly, intercell access to mutually matching interaction partners presented on the bacterial exterior. They also facilitate the predictive modeling of multistrain assembly formation in tridimensional flocks embodying artificial communities or forming structured catalytic consortia.

RESULTS AND DISCUSSION

Identifying Genetic Determinants to Obtain a Surface-Naked Variant of *P. putida* KT2440. We started by an *in silico* analysis of the genome of *P. putida* KT2440[33] and identified a nonexhaustive set of 21 regions/operons encoding elements that may be exposed on the bacterial surface. Within these DNA regions, we included fimbriae, surface adhesion proteins, exopolysaccharides, the O-antigen side chain, the flagella, and other conspicuous envelope-associated components. These regions are distributed throughout the genome of the strain under examination (Figure 1A). The construction of a surface-naked variant followed a specific roadmap in which the selected DNA regions were sequentially removed from the genome using a homologous recombination-based approach that generates scarless deletions.[34,35] The specific order for the serial deletion steps followed to construct the target strain is sketched in Figure 1B and Table S1. Broadly speaking, we clustered these regions into four groups: [i] complex structures, [ii] surface proteins, [iii] regions related to production of extracellular polymeric substances (EPSs), and [iv] other, non-OM-associated elements.

Within the complex structures group, we have two regions that encode putative fimbrial-like structures, the *PP_1887-PP_1891* cluster and the *csu* operon (*PP_2357-PP_2363*).[36−38] There are also several loci that encode putative type IV pili genes and a pilus chemotaxis locus (*PP_0607-PP_0611*; *PP_1993*; *PP_5080-PP_5083*; *PP_5093*; and the *PP_4986-PP_4992*, respectively). These elements allow attachment to surfaces, aggregation, and twitching motility.[39] In addition, we deleted the entire flagella operon (*PP_4329-PP_4397*).[40] The last element of this group is the O-antigen, located at the most distal part of the complex and

https://dx.doi.org/10.1021/acssynbio.0c00272
ACS Synth. Biol. 2020, 9, 2477−2492

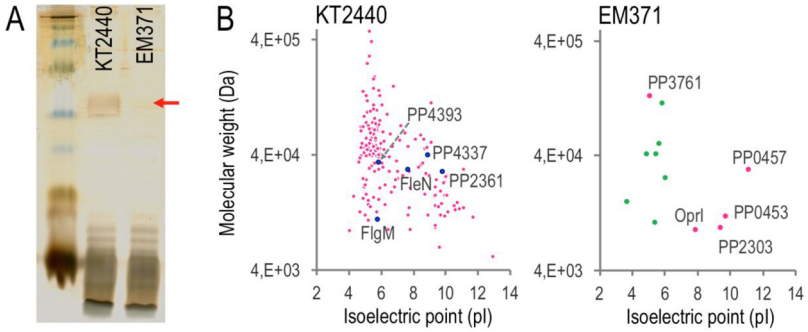

Figure 2. Surface properties of the surfome-streamlined strain. (A) Silver stained SDS−PAGE used to analyze the pattern of LPS (represented by a red arrow in the image) in KT2440 and EM371 of whole cell lysates. Kaleidoscope prestained standard (BioRad, CA, USA) was used as the marker. (B) Surface-associated proteins captured by activated magnetic nanoparticles in *P. putida* KT2440 and EM371. Cells were treated with activated nanoparticles (NPs) to capture envelope-associated proteins that were identified through MudPIT analysis. Each identified protein is represented in a virtual 2D map by a colored point defined by its theoretical isoelectric point (pI) and molecular weight (MW). In the chart of KT2440, blue dots correspond to proteins deleted in the naked strain. In the case of EM371, pink dots correspond to five proteins also identified in the parental strain KT2440, while green ones represent proteins identified only in the naked strain.

multidomain lipopolysaccharide (LPS) molecule. The O-antigen is composed of repeated oligosaccharides producing a side chain of variable length; it has a protective role, is important in cell adhesion and surface attachment, and is also highly immunogenic.[41,42] Previous works identified that *P. putida* has only the high molecular weight B-band form,[43,44] and in KT2440, the transmembrane glycosyltransferase *wbpL* starts the assembly of the O-antigen side chain of LPS; mutations in that gene interrupted its synthesis.[44] Therefore, we deleted the *wbpL* gene (*PP_1804*) to eliminate its synthesis and, with it, also removed the last 4 bp of the upstream gene *wbpV*.

Within the second group, we selected three regions that encode large surface adhesion proteins *PP_0164-PP_0168*, *PP_0803-PP_0806*, and *PP_1449-PP_1450*.[45] Within the cluster *PP_0164-PP_0168* lies the largest gene in the genome of KT2440 that encodes LapA (*PP_0168*) a key factor for adhesion to corn seeds[46] and plant roots.[47] LapA is directed to the surface by the ABC transporter composed of LapCBE (*PP_0166-PP_0167-PP_4519*).[48] This cluster also comprises a c-di-GMP-binding protein (LapD)[49] and a periplasmic cysteine protease (LapG).[50] Thus, we made a clean deletion of the whole *PP_0164-PP_0168* cluster. We also deleted the cluster *PP_0803-PP_0806* containing the second largest surface protein LapF (*PP_0806*) and a proper ABC transporter (LapHIJ). LapF is in charge of microcolony formation by providing cell-to-cell interactions that prompt the formation of mature biofilms, and it is also important in the colonization of biotic and abiotic surfaces.[51] We also selected the operon *PP_1449-PP_1450* that encodes a two-partner secretion (TPS) system involved in seed colonization and iron uptake.[52] Within the operon, the protein HlpA (*PP_1449*) looks like a filamentous hemagglutinin adhesin, and it is predicted to be either localized on the cell surface or secreted. Moreover, we included a putative outer membrane lipoprotein (*PP_1131*), an operon *PP_2891-PP_2893* encoding a putative surface antigen D15, and also the locus *PP_1879-PP_1882* that encloses a putative outer membrane autotransporter and a large RHS element containing YD-peptide repeats.

In the EPS-related group, we included exopolysaccharides and curli fibers produced by bacteria under diverse environmental conditions that have different physiological roles such as maintaining the integrity of the cell envelope, preventing desiccation, and colonizing surfaces by providing structural support for biofilms in many bacteria.[53] Within the genome of KT2440 there are several loci involved in the production of different types of exopolysaccharides.[45,54] Of these, there is the bacterial cellulose synthesis (*bcs*) operon (*PP_2629-PP_2638*). Cellulose is an extracellular polymer composed of D-glucose monomers linked by β-1,4 glycosidic bonds and is key for cell adherence, for the provision of structural support to biofilms, and for the colonization of the rhizosphere.[55,56] In a similar way, the *pea* locus (*PP_3132-PP_3142*) encodes a cellulase-sensitive polysaccharide that has a role in stabilizing biofilms.[54,56] Another important polysaccharide that is commonly found in the EPS matrix of bacteria is alginate, which is composed of *o*-acetylated β-1,4-linked D-mannuronic acid and α−L-guluronic acid.[57] Previous reports indicated that *P. putida* produces alginate under water limitation stress in order to reduce the water loss in biofilms helping to preserve a hydrated environment and also helping to offer protection against reactive oxygen species (ROS) generated due to matric stress.[58,59] KT2440 contains two *alg* operons, one with structural genes (*PP_1277-PP_1288*) and another with regulatory elements and the alternative sigma factor (RpoE or AlgU) (*PP_1427-PP_1430*), which control not only alginate production but also manage cell envelope stresses.[57] Furthermore, the proteinaceous amyloid-like fibrils known as curli play an important role in the colonization of surfaces and in the scaffolding of biofilms.[60] The genome of KT2440 bears two clusters with components related to the synthesis and export of curli. The *PP_3396-PP_3399* operon bears the major (CsgA-like) and minor (CsgB-like) curli subunits, where the second locus *PP_3472-PP_3484* encodes nonstructural genes involved in curli biogenesis and secretion.

Within the last group, we included an element not related to the OM (the Tn7-like transposase operon *PP_5404-PP_5407*[18]) in order to increase the stability of recombinant strains engineered using this minitransposon.[61,62] In addition, we realized that, during the course of constructing this deep engineered strain, prophage 4 (*PP_1532-PP_1584*) was spontaneously lost from the genome due to a natural excision event[63] that occurred sometime after deletion no. 18 (Figure S1A). As a consequence of that, the resulting variant is more resistant to UV than the parental strain[63] (Figure S1B).

https://dx.doi.org/10.1021/acssynbio.0c00272
ACS Synth. Biol. 2020, 9, 2477−2492

Eventually, the surface-streamlined strain encompassed 23 deletions that include a total of 235 genes. The genomic coordinates and the precise extension of each deletion, based on the reference genome of *P. putida* KT2440 (GenBank no.: AE015451[45] and AE015451.2[64]), are compiled in Table S1. Diagnostic PCRs were performed to confirm deletions using oligonucleotides that hybridize within the excised region (Table S2 and Figure S1C). Also, the predicted boundaries of each deleted region were PCR amplified and the flanking regions sequenced. All of these deletions accounted for an ∼4.7% genome reduction size of the parental strain. This surface-naked variant of the wild type strain was designated as *P. putida* strain EM371. The following sections describe its phenotypic and physiological properties as well as its value for ectopic display of artificial adhesins closely bound to the cell's exterior layer.

Envelope-Edited *P. putida* EM371 Strain Displays a Simplified Outward-Facing Molecular Landscape. One characteristic external structure that cells expose to the outer environment is the LPS. We started by checking whether the deletion of the O-antigen glycosyl transferase (*wbpL*) correlates with the absence of this exposed structure in the *P. putida* EM371 strain. To this end, we extracted lipopolysaccharides from the wild type and the naked strain, separated them by an SDS−PAGE, and visualized them by silver staining. As expected, the surface-edited bacteria lack the typical ladder pattern that correspond with the high molecular weight of the repeating polysaccharide (Figure 2A). This result confirms the absence of this complex structure in *P. putida* EM371. Along the same line, we compared whether there were differences in the whole of the surface-exposed proteins (surfome,[65−67]) detected in the parental and in the naked strains. To do this, we used an experimental approach based on the use of activated magnetic nanoparticles (NPs) combined with a multidimensional protein identification technology (MudPIT).[68] Briefly, small iron oxide nanoparticles (70−90 nm of diameter) covered with carboxymethyl dextran were chemically activated and mixed with intact whole cells, as explained in the Methods section. Then, NPs attached to bacteria were magnetically purified, and the bound proteins were identified by MudPIT. Proteins considered bound by NPs at the cell surface were identified, because the corresponding average spectral count (SpC) resulted in a significantly higher value than the SpC determined with the shedding controls (see Methods for details). This technology identified a total of 196 surface-presented proteins in the parental strain, while in the case of the surface-naked variant, only 12 could be recognized (Figure 2B and Table S3). Among these, only five proteins were identified as being shared by both strains. Moreover, within the proteins recognized in KT2440, those conspicuously present in the wild type strain but missing in *P. putida* EM371, as expected, included four components of the flagellar operon and one constituent of type I fimbriae. Moreover, the pool of proteins covalently bound by NPs at the cell surface in KT2440 included typical outer membrane (OM) components such as the lipoproteins OprL and OprI, the porin OprD, OprH, and an OmpA family protein (Table S3). More surprisingly, a number of proteins predicted to localize in the inner membrane (IM) did appear as surface-exposed proteins in the MudPIT data of Table S3. As shown in other surfome studies in Gram-negative bacteria,[68] this is not entirely unknown, as many proteins predicted to localize in the inner membrane (IM) do occasionally appear to be associated with the OM as well. Although technical issues cannot be ruled out, it is also possible that such proteins may reach out beyond the IM and even protrude outward. Such a notion may also be true for a number of proteins of Table S3, which do appear on the cell exterior despite being predicted or experimentally determined earlier within the IM. In other cases, classical cytoplasmic proteins, such as ribosomal proteins, along with other anchorless products, have been observed on bacterial surfaces in a variety of studies.[69−72] Data shown in Table S3 also include some proteins typically considered cytoplasmic. Nonoverlapping examples of these appeared both in the wild type strain and the surface-edited counterpart, and interestingly, seven of them, *i.e.*, PP_5354 (cell wall assembly protein), PP_5001 (ATP-dependent protease ATP-binding subunit HslU), PP_3431 (ThiJ/PfpI domain-containing protein), PP_2410 (cobalt−zinc−cadmium resistance protein CzcA), PP_1989 (aspartate−semialdehyde dehydrogenase), PP_1360 (cochaperonin GroES), and PP_0856 (outer membrane protein assembly factor BamB), were detected at the surface of *P. putida* EM371 and not in the parental strain. By the same token, there are proteins observed in the wild type KT2440 strain and not in *P. putida* EM371 although their genes were not deleted. How could these happen? Specific mechanisms accounting for the observed protein misplacement cannot be ruled out, but it could also happen that alteration of the charge distribution on the cell surface caused by the deletions changes the profile of proteins captured by the NPs through mere electrostatic interactions. One way or the other, the drastic change in surfome composition and the O-antigen loss undergone by *P. putida* EM371 (Figure 2) causes a major simplification of the molecular landscape that can be encountered when approaching cells from the outside.

Coarse Physiological and Morphological Analysis of the Surface-Streamlined Strain. The next step in the characterization of *P. putida* EM371 was the comparison of its physiological vigor with that of the wild type strain. This was made by assessing growth physiology on different carbon sources that establish different metabolic regimes: LB for rich medium and in M9 minimal medium with either a gluconeogenic (succinate) or glycolytic (glucose) carbon source. Bacterial growth was monitored by following the OD_{600} in a 96-well plate for 24 h. Figure S2A shows the overall growth profiles of both strains with the different media under examination. There was a significant alteration in the growth rate of both strains in nutrient-rich medium, while there is no significant difference when growing them in minimal media supplemented with either a gluconeogenic or a glycolytic carbon source. On the other hand, the total optical cell density reached with this experimental setup constraints the capacity of *P. putida* EM371 due to the combined effect of the limited aeration in a plate reader together with the absence of flagella in this strain. To clarify this, we regrew cultures in Erlenmeyer flasks with vigorous shaking and measured the OD_{600} at 24 h. Under these conditions, the *P. putida* EM371 strain reached similar OD_{600} values in LB and M9 glucose, while less total growth was achieved in M9 succinate (Figure S2B). This fact might be due to the effect of changes of surface hydrophobicity (see below) on transport of dicarboxylates, an issue that deserves clarification.

Because many of the elements deleted in *P. putida* EM371 may have a deep impact on the social behavior and on the cellular and macrocolony morphology of this strain, we next inspected these traits. Flagellum, the locomotion organelle, is

https://dx.doi.org/10.1021/acssynbio.0c00272
ACS Synth. Biol. 2020, 9, 2477−2492

used to propel bacteria in a nonsocial manner to explore and scavenge nutrients in the environment.[73] We analyzed the swimming ability of the strains of interest in soft agar plates where cells are able to penetrate the matrix and move through the medium,[74] thereby generating a halo that surrounds the inoculation spot. As shown in Figure 3A, when cells were

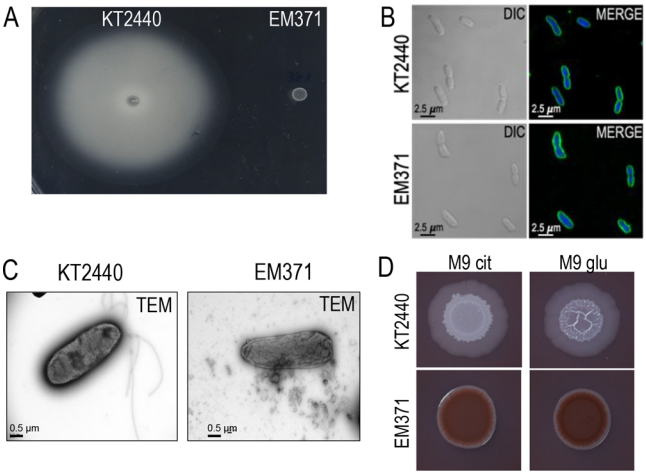

Figure 3. Motility test and cell and colony morphologies of *P. putida* wild type and EM371 surface-naked strain. (A) Swimming ability of KT2440 and EM371. Cells grown overnight were spotted on M9-glucose semisolid agar plates, incubated at 30 °C for 48 h, and photographed. (B) Nucleic acids and membrane staining of *P. putida* KT2440 and EM371. Cells were stained with the membrane dye FM1-43FX, and DNA was stained with DAPI and visualized with DIC and the appropriate fluorescence channels in a confocal microscope. The FM1-43FX (colored in green) and DAPI (blue) channels were merged and represented. (C) Electron microscopy images of the parental and naked strains. Samples were negatively stained with uranyl acetated and observed with a JEOL JEM 1011 transmission electron microscope. (D) Macrocolony morphology assay. Bacterial samples were spotted on M9 minimal medium supplemented with either citrate or glucose as the sole carbon source and with Congo Red and Coomassie Brilliant Blue; they rested at 30 °C for 3 days and were photographed.

placed on an M9-glucose 0.3% (w/v) agar plate, deletion of the flagellar operon in the *P. putida* EM371 strain rendered nonmotile cells. Morphology of individual bacteria was next examined by fluorescence microscopy. For a better visualization, cells were stained in the first case with both the membrane dye FM1-43X (that produces a strong fluorescent emission in hydrophobic environments) and DAPI (that specifically binds DNA). The differential interference contrast (DIC) and merged fluorescence images (FM1-43X + DAPI) obtained are shown in Figure 3B. Both strains showed similar morphologies, and the specific membrane dye stained both cells, likewise. To obtain a closer look into the cellular morphology and also to confirm the absence of deleted outer membrane structures, we also used transmission electron microscopy (TEM) of negatively stained bacterial samples. In the pictures obtained, the flagellum is clearly visible only in the wild type strain while the multideleted engineered strain is nonflagellated (Figure 3C), as confirmed previously in the swimming assay.

Finally, colony morphology of the surface-naked strain was inspected as well. When bacteria grow on solid surfaces they form complex 3D multicellular structures resulting from production of a diverse number of elements commonly known as the extracellular polymeric substance (EPS), which includes exopolysaccharides, pili, adhesins, and curli, among others. The deletion of many of these elements in *P. putida* EM371 prompted us to explore the macrocolony development of this strain. To this end, we used M9 minimal medium with either citrate or glucose as C-source and Congo Red and Coomassie Brilliant Blue as generic dyes for exposing EPS production. These chemicals bind a number of extracellular matrix components such as amyloid fibers (curli), fimbriae, and cellulose.[75,76] For the assay, we spotted 5 μL of cells grown overnight onto agar plates containing the dyes and incubated them for 3 days at 30 °C. As expected, the EM371 strain developed flat and smooth colonies, while *P. putida* KT2440 gave rise to more complex, elaborated, and wrinkled structures, especially with glucose as the C-source (Figure 3D). In contrast, *P. putida* EM371 rendered intense red colonies, while the wild type strain produced much paler colors (from pink to white). These differential phenotypes could be be caused by variations in the internal cyclic-di-GMP levels brought about by the resetting of the cognate regulon.[9,77,78] However, it could also be traced to different affinities to the dyes due to altered properties of the envelope or even due to an increased self-aggregation of the engineered strain. To shed some light on these possibilities, we next studied changes in the material characteristics of *P. putida* EM371's envelope, which were caused by the deletion of surface structures.

Sedimentation, Surface Hydrophobicity, and Membrane Permeability. Deletion of flagella is known to influence the bacterial sedimentation rate and surface hydrophobicity of *P. putida*.[40] On this basis, we tested how nonshaking growth conditions affect sedimentation of the engineered strain. To do that, we incubated overnight cells two grow without any agitation for 24 h at room temperature (RT) and measured the OD_{600} of the top part of the test tube. As observed in Figure 4A, the surface-naked strain not only settled at the bottom of the tube, but it did so more pronouncedly than cells simply lacking the flagella.[40] In order to determine whether this was the result of changes on cell surface hydrophobicity, we next tested how the deletion of multiple outer membrane structures entered in the *P. putida* EM371 strain such as flagella, surface proteins, LPS, *etc.*, affected such a physical parameter. For this, we performed a comparative microbial adherence to hydrocarbon (MATH) test[79,80] with the wild type and the naked strains. This procedure measures the affinity of the bacterium to an organic phase (alkane) as a proxy of the overall hydrophobicity of the bacterial surface. The more hydrophobic the cell surface is the more bacteria partition to the organic layer, and this is reflected with a higher MATH score. Not surprisingly, the naked strain showed a much less hydrophobic surface than that of the parental strain ($P < 0.0001$ unpaired *t*-test; Figure 4B). This finding is consistent with earlier observations, the effect of lacking the flagella and of the LapF protein on cell surface hydrophobicity,[40,81] and accounts for the differential tendency to sedimentation shown in Figure 4A.

Deletion of the different outer membrane structures could also affect the overall permeability of the cell envelope. To check this possibility, we further inspected whether the surface of the naked strain had the permeability altered using the simple and visual protocol described in ref 82. Briefly, this method relies on the use of a galactoside analogue (chlorophenol red-β-D-galactopyranoside; CPRG) that pro-

https://dx.doi.org/10.1021/acssynbio.0c00272
ACS Synth. Biol. 2020, 9, 2477−2492

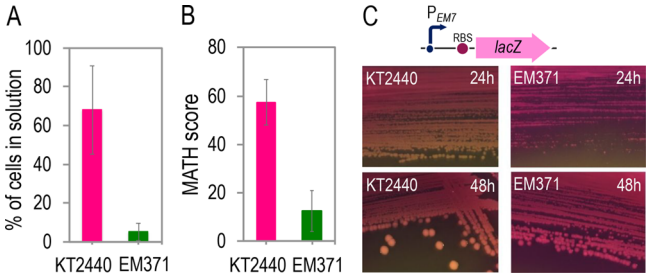

Figure 4. Sedimentation, hydrophobicity, and permeability of *P. putida* EM371 cells. (A) Sedimentation assay of KT2440 and EM371. Overnight grown cultures in 4 mL of LB (OD_{600} value set to 100%) were incubated without agitation at room temperature for 24 h, and the OD_{600} from the upper part of the test tube was measured to calculate the percentage of cells persisting in solution for each strain. The average and standard deviation of five experiments are shown. (B) Surface hydrophobicity scores for KT2440 and EM371. The microbial adhesion to hydrocarbon (MATH) experiment was performed with exponential cells washed with the PUM buffer, and their adhesion to hexadecane was determined to calculate the MATH score as $(1\text{-}OD_{600}^{final}/OD_{600}^{initial}) \times 100$. The average and standard deviation of six experiments are shown. (C) Permeability test by using CPRG indicator agar plates. On top, there is a schematic representation of the construct used to constitutively express the LacZ enzyme in the *P. putida* strains at stake. Cells, harboring plasmids with the above-mentioned operon, were streaked on LB agar plates supplemented with 20 μg mL^{-1} CPRG and incubated for 24 h and 48 h at 30 °C.

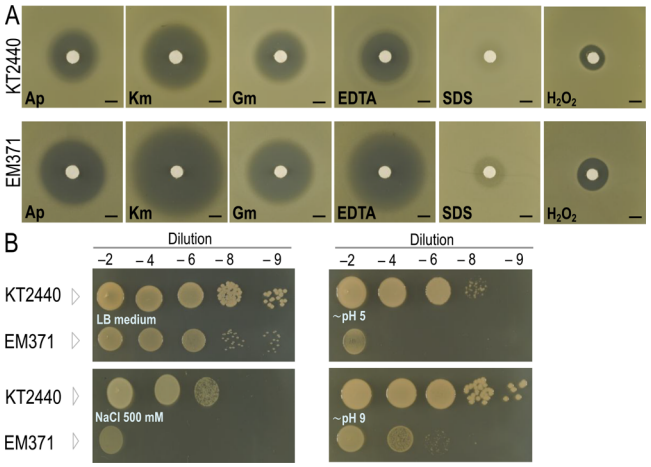

Figure 5. Effect of different stressors on *P. putida* KT2440 and the surface-naked strain. (A) Overnight grown culture (100 μL) was added to soft agar and spread onto an LB agar plate. Then, a sterile filter disk was spotted on the plate and soaked with 10 μL of the specific chemical: 150 mg mL^{-1} Ap, 50 mg mL^{-1} Km, 10 mg mL^{-1} Gm, 0.5 M EDTA, 10% (w/v) SDS, and 30% (v/v) H_2O_2. Plates were incubated for 24 h at 30 °C and photographed. The area that contains the inhibition halo is blown up. The black scale corresponds to the diameter of the filter disk (~0.5 cm). (B) LB grown cultures were serially diluted and spotted onto LB agar plates supplemented with the different stressors. Plates were incubated overnight at 30 °C and pictured.

duces a visible red color compound (chlorophenol red, CPR) when degraded by the cytoplasmic LacZ enzyme. Given that CPRG cannot enter cells directly, the dye becomes colored only with an increased surface permeability. Because *P. putida* lacks an endogenous β-galactosidase enzyme, we transformed the strains under scrutiny with high/medium copy plasmid pSEVA2513-LacZ (Table S4), which bears the *E. coli lacZ* gene expressed from the P_{EM7} constitutive promoter. Transformants were then streaked on LB + Km agar plates supplemented with 20 μg mL^{-1} CPRG, incubated, and photographed after 24 and 48 h of growth at 30 °C. Figure 4C shows that the biomass of the surface-naked strain has a pinkish-red color, while parental *P. putida* KT2440 produces whiter colonies at either incubation time. This suggests that *P. putida* EM371 had a more permeable cell envelope that allows CPRG to enter cells and reach the plasmid-encoded β-galactosidase. This increased permeability may account for the red colonies that develop in media with Congo Red/Coomassie Blue strain shown in Figure 3D.

Stress Resistance Profile of the *P. putida* EM371 Strain. The evidence about having a more permeable envelope prompted us to test whether this was translated into increased sensitivity to archetypal stressor compounds. To examine this, we exposed cells to a number of drugs and chemicals that elicit distinct types of insults and evaluated bacterial tolerance to them by simply recording the inhibition halo caused by each specific compound (Figure 5A). The stress response was estimated using soft-agar experiments in which a molten 0.7% (w/v) LB agar suspension containing the bacterial cells was spread onto LB agar plates. Sterile filter disks were placed on top of the bacterial lawn and soaked with the specific stressor, after which plates were incubated overnight at 30 °C. Among the compounds assayed, we included the β-lactam ampicillin (disrupts the cell wall by interfering with the peptidoglycan synthesis) and the aminoglycosides kanamycin and gentamicin (which inhibit protein synthesis). Note that ampicillin is a zwitterionic drug that uses porins as the conduit to cross the OM, while aminoglycosides are polycationic and hydrophobic antibiotics that gain access to the cytoplasm by permeation through the double-layered envelope.[83] We also exposed cells to the chelating agent EDTA, the denaturing anionic detergent SDS, and the oxidative agent H_2O_2. In general, as shown in Figure 5A, the naked strain turned out to be more sensitive to all stressors tested. The most pronounced effects were observed with the most hydrophilic ones (based on the octanol/water partition coefficient, see above), namely, Km and EDTA. This confirmed that the increased permeability of the envelope of the naked strain translates into a more stress-susceptible strain. Moreover, the naked strain was also more sensitive to the redox stress caused by H_2O_2 suggesting lower levels of reducing power available in *P. putida* EM371 to counteract the ROS produced by the oxidative damage.[84] Finally, we also investigated whether high osmotic conditions and exposure to acidic and basic pH values affected the viability of the surface-naked strain. In this case, cells from cultures grown overnight were serially diluted and spotted onto LB agar plates with either divergent pH values or a high salt content. As observed in Figure 5B, the surface-naked strain was also more sensitive to all of these stresses, in particular, to osmotic challenge and acidic pH. Although all these tests were qualitative, taken together, they expose the degree of physiological trade-off between having an outer envelope more exposed to the environment and the increased vulnerability to external insults.

Autoaggregation of *P. putida* EM371 Depends on Cell Surface Solvation. In view of the observations above (autoaggregation visible with the naked eye, alteration of surface hydrophobicity, increased permeability, and sensitivity

https://dx.doi.org/10.1021/acssynbio.0c00272
ACS Synth. Biol. 2020, 9, 2477−2492

to stressors), we wondered whether this behavior could be influenced by the additives in growth media that act as solutes for solvation of the bacterial envelope. The salt (NaCl) concentration of LB medium varies among recipes from 5 g L^{-1} (85.5 mM) LB-Lennox to 10 g L^{-1} (171.1 mM) LB-Miller or even to 0.5 g L^{-1} (8.5 mM) LB-Luria. Note that the differences in ionic strength caused by such salt concentrations are significant. Because salt concentration does influence flocculation of bacteria in liquid cultures,[85] we tested whether different NaCl contents in the growth media modified the tendency of *P. putida* EM371 to quickly sediment. To this end, we grew the wild type and surface-naked strain in LB with concentrations of NaCl ranging from 0 to 400 mM,[86] let them grow overnight, and measured the A_{600} of the liquid culture with and without vortexing. The corresponding ratio (A_{600}-vortex/A_{600}-no vortex) was considered an indication of the total number of cells *vs* the share of them that aggregated; *i.e.*, the bigger the ratio the more flocculation in the culture. Figure 6A shows that increasing NaCl in the growth media favored

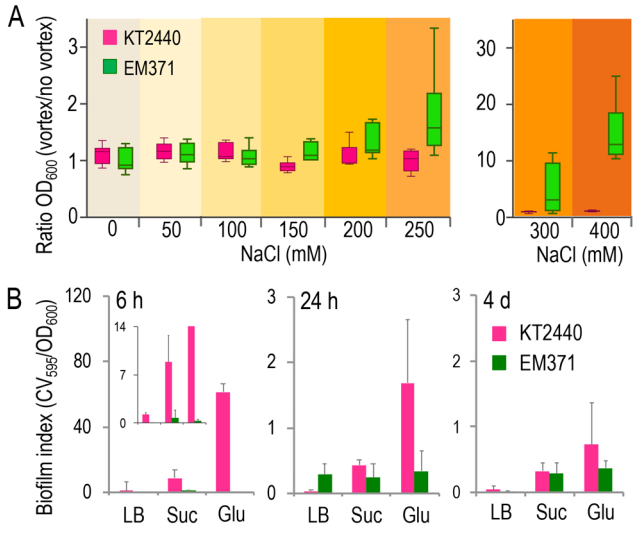

Figure 6. Aggregation and biofilm formation of *P. putida* with an edited surfome. (A) Influence of NaCl in the growth physiology of KT2440 and EM371 strains. Cells were grown on LB without and with different NaCl concentrations overnight with 170 rpm at 30 °C. Then, the OD_{600} of cultures measured before and after vortexed the tubes to disrupt flocks. The OD_{600}-vortex was divided by the OD_{600}-no vortex, and the obtained values of six experiments are represented as a Tukey box-and-whisker plot. The pink color is for KT2440, while green is for EM371. (B) Biofilm index after 6 h, 24 h, and 4 days of KT2440 (pink) and EM371 (green) in different media: LB as rich media and M9 minimal media with either 0.2% (w/v) succinate (Suc) or glucose (Glu) as the C-source. Biofilm index was calculated as the ratio of crystal violet staining (CV_{595}) to the OD_{600} of the culture. Within the 6 h chart, a zoomed in inset has been included to better visualize the biofilm response of both strains at lower values. The average and standard deviations of three experiments are shown.

aggregation of the surface-naked bacteria. In contrast, such salt-dependent sedimentation was not observed in the parental strain. Because solvation of the cell surface allows particles/bacteria to remain suspended in liquid media, this phenomenon is likely to reflect the cumulative result of the absence of the O-antigen and other exposed proteins in the interactions of charged sites of the envelope with salt ions. Such surface structures contribute to solvation of the cell envelope of the parental strain. In contrast, the observed autoaggregation of *P. putida* EM371 plausibly reflects a phase separation phenomenon similar to the salting-out effect of proteins.[87] In this case, particles of amphiphilic behavior are segregated from the solvent by increasing the ionic strength of the medium. Under this scenario, increasing the NaCl concentration fosters cell clumping by hydrophobic interactions, as the solvating power of the surface of the *P. putida* EM371 strain would not be strong enough to thermodynamically stabilize cells in solution and counteract this effect.[88−90] The practical consequence of all this is that surface-naked cells can be made more or less stable in suspension by manipulating salt contents of the growth media.

Attachment of Surface-Naked Bacteria to Solid Supports. The next step in the characterization of *P. putida* EM371 involved inspection of whether this strain attached to abiotic surfaces and could establish biofilms. Because the surface-naked variant lacks elements that are crucial for bacterial adhesion and biofilm development, we expected a reduction of this capacity in comparison with that of the parental strain. To test this, we analyzed biofilm formation at different physiological states and with various growth media to cover a broad number of conditions. Biofilm formation was analyzed through the classical crystal violet assay[91] using three different time points that represent the initial (6 h), middle (24 h), and latter (4 days) stages of the process. We also compared biofilm formation in three different growth conditions: rich medium (LB), gluconeogenic (M9 + succinate), and glycolytic (M9 + glucose). As shown in Figure 6, the surface-naked strain did not form as much apparent biofilm as that of the wild type in any of the conditions tested, especially at the initial stages of biofilm formation (6 h). At this time, flagella initiate the attachment process followed by the action of pili, surface proteins, and EPS to complete the formation of the biofilm structure.[91,92] At the 24 h time point, the naked strain produced less biofilm than the wild type bacterium in minimal media. In contrast, *P. putida* EM371 remained stably stuck to solid surfaces in LB medium. This phenomenon could be due to the flagella-mediated disengagement of *P. putida* KT2440 cells from matured biofilm to colonize new niches.[93,94] In this case, the surface-naked cells could not escape from their initial landing pad, thereby remaining in a sessile form. The tendency remains after 4 days; by that time, the wild type cells have gone through all phases of biofilm development, while the surface-naked cells display a low capacity of adhesion to the wells throughout the whole timeline of the experiment. In fact, it is very unlikely that *P. putida* EM371 forms *bona fide* biofilms at all: What we see as crystal violet stainable biomass is likely to be an amorphous aggregate rather than a typically 3D-structured bacterial population. Once these qualities of the surface-naked strain were set, we moved on to the ultimate tests for assessing accessibility of the outward-facing cell envelope to exterior actors.

Displaying Heterologous Autotransporters with Fos and Jun Interacting Partners in *P. putida* EM371. As mentioned above, one key motivation for constructing a surface-naked strain was to facilitate the display of molecules on the bacterial body and thus modify adhesion properties *a la carte*. To test the value of the *P. putida* EM371 strain, we recreated, in *P. putida*, the protein display system described for *E. coli* by ref 11. This approach consists of the production of a hybrid polypeptide containing the β-domain of the immunoglobulin A protease from *Neisseria gonorrheae* (IgAβ) fused to

https://dx.doi.org/10.1021/acssynbio.0c00272
ACS Synth. Biol. 2020, 9, 2477−2492

the eukaryotic leucine zipper transcriptional factors Fos or Jun. In that way, the IgAβ crosses the inner membrane thanks to the presence of the *pelB* signal peptide (SP) at the N-terminal of the hybrid protein, and the β-domain integrates in the outer-membrane, thereby exposing the Fos or Jun molecules to the external medium. These leucine zippers tend to interact through the coiled coil domains of their structure and produce heterodimers (also the Jun molecules could interact with each other, producing homodimers[95]). On this basis, we cloned the Fos-E-tag-*igA*β and the Jun-E-tag-*igA*β modules into the broad host range expression vector pSEVA238 to obtain plasmids pSEVA238-AT-Fos and pSEVA238-AT-Jun (Table S4). As an intracellular expression control, we cloned the hybrid nanobody Trx-$^{G6}V_{HH}$ from ref 96 into the same backbone to yield plasmid pSEVA238-trx-$^{G6}V_{HH}$ (Table S4). A schematic representation of the business parts of these three plasmids is shown in Figure 7A. They were then introduced into the

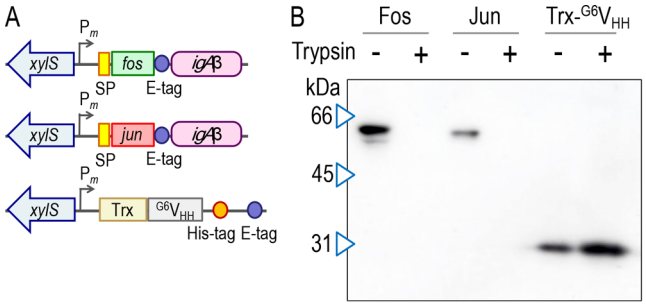

Figure 7. Organization, expression, and localization of the Fos and Jun chimaeric proteins. (A) Schematic representation of the constructs used for surface display in *P. putida*. The Fos and Jun leucine zipper domains preceded by the *pelB* signal peptide sequence (SP; yellow) and together with an E-tag epitope (blue circle) and the *igA*β module as the transporter module (purple) were placed under control of the *xylS*-P_m expression system of pSEVA238.[27] As a cytoplasmic expression control, we used a construction cloned into the same expression pSEVA238 plasmid containing a thioredoxin domain (Trx) fused to the $^{G6}V_{HH}$ nanobody followed by the His-tag and E-tag epitopes. (B) Western blot of extracts of induced whole cells of EM371 with pSEA238 plasmids containing either the Fos-*igA*β, Jun-*igA*β, or Trx-$^{G6}V_{HH}$ hybrid proteins. Also, induced cells were treated (+) or not treated (−) with trypsin. The Western blot was revealed with anti-E-tag as the primary antibody and with antimouse IgG conjugated with peroxidase.

fluorescently-tagged variants of the naked strain (nonlabeled, GFP, and mCherry; Table S4), and expression of hybrid proteins Fos-*igA*, Jun-*igA*, and Trx-$^{G6}V_{HH}$ was induced upon addition of inducer 3-methyl-benzoate (3MBz) to the growth medium. *In vivo* expression and cellular localization were then monitored owing to the E-tag epitope engineered in the fusions (Figure 7A). Figure 7B shows the Western blot corresponding to extracts of whole induced cells of the surface-naked strain treated (+) or not treated (−) with a protease (trypsin). This enzyme cannot penetrate intact cells and thus degrades only exposed and accessible proteins.[97,98] The Western blot result of Figure 7B shows that the hybrid Fos-*igA* and Jun-*igA* are expressed in the surface-naked strain (~54 kDa) and that both are clearly located on the cell exterior, because those bands disappeared after the treatment with trypsin. In the case of cells bearing the control plasmid with an intracellular protein, expression (~29.5 kDa) is observed independently or not of trypsin treatment. Figure S3A shows that the cytoplasmic control construct (Trx-G^6V_{HH}) is not degraded by the protease unless cells are made permeable with lysozyme. Note that the effect of the enzyme was verified by immunofluorescence (Figure S3B). When the same plasmids were placed in the parental strain *P. putida* KT2440, correct expression and surface localization of Fos-*igA*, Jun-*igA*, and Trx-$^{G6}V_{HH}$ could be verified as well (Figure S4). However, this data does not tell us by themselves how easily the exposed Fos and Jun moieties of the hybrid proteins are accessed from the cell's outside in each strain. To test this, we resorted to a simple test for detecting surface-to-surface contacts, as explained below.

Conditional Flocculation of *P. putida* upon Expression of Surface-Displayed Synthetic Adhesins. To have an estimation of accessibility of *P. putida* surfaces under various conditions, we developed the aggregation test shown in Figure 8A. Green-tagged and red-tagged *P. putida* cells expressing Fos-E-tag-*igA*β and Jun-E-tag-*igA*β were mixed in a 1:1 ratio, and production of the corresponding proteins was induced with 3MBz. The rationale of the experiment is that display of the matching interacting partners should bring about cell-to-cell-specific interactions that grossly manifest as aggregates of different sizes within the culture. As shown in Figure S5, the aggregation caused by expression of the artificial adhesins (F−J and J−J) in *P. putida* EM371 became evident when inspected in detail with confocal microscopy.

In order to parametrize the effect of the surface editing made in the naked strain, we developed an algorithm for inspecting, quantitatively, microscope images, including physical identification and counting of either bacterial aggregates ($n > 2$; in order to exclude possible dividing cells) or singlets ($n \leq 2$) in each condition (Figure 8B). Aggregation data were then generated by inducing cultures containing equal amounts of either *P. putida* EM371-GFP (Fos-*igA*) or *P. putida* KT2440-GFP (Fos-*igA*) with either *P. putida* EM371-cherry (Jun-*igA*) or *P. putida* KT2440-cherry (Jun-*igA*). Samples were then observed under confocal microscopy, and the percentage of cells forming aggregates *versus* singlets was automatically quantified. Figure 8C shows representative pictures of strains *P. putida* EM371 and *P. putida* KT2440 with the Fos and Jun expressing plasmids as well as the same strains without the adhesins. The resulting quantification indicated that 84% of *P. putida* EM371 cells expressing Fos-*igA* and Jun-*igA* formed *bona fide* aggregates, while those formed by adhesinless bacteria went down to 54%. In the case of the wild type strain *P. putida* KT2440, the percentage of aggregates mediated by adhesins was 27%, while spontaneous clumping came down to 9% (Figure 9A). Furthermore, *P. putida* EM371 cells expressing adhesins resulted in aggregates containing more bacteria on average ($n = 5$) than in any of the other cases (Figure 9B and Figure S6). Despite the above-discussed tendency of the *P. putida* EM371 strain to flocculate naturally, expression of artificial adhesins enhanced cellular aggregation by a factor ≥ 1.8 (Figure 9C). On this basis, we estimated that external approachability of the cell surface nearly doubled after stripping the bacterial envelope of all structures listed in Figure 1.

CONCLUSION

While the value of *P. putida* KT2440 and its derivatives as a platform for metabolic engineering and a synthetic biology chassis is well accredited,[24,31] there is still much room for improving its performance through engineering physical, not

https://dx.doi.org/10.1021/acssynbio.0c00272
ACS Synth. Biol. 2020, 9, 2477−2492

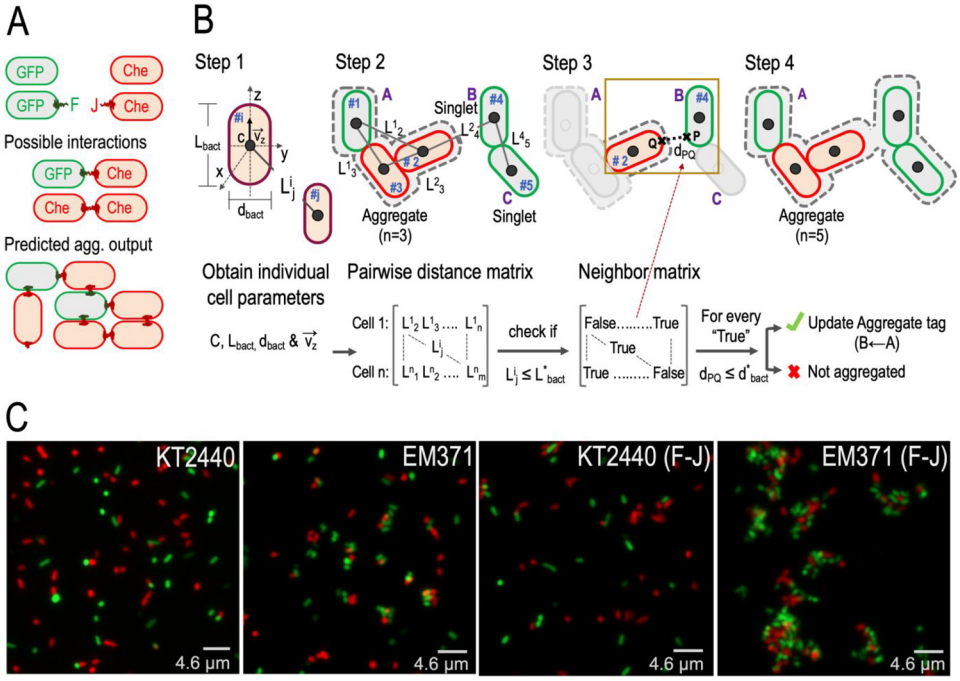

Figure 8. Modeling and visualizing *P. putida* cell−cell adhesion. (A) Predicted possible bacterial pair interactions between strains expressing either Fos and Jun or Jun and Jun. KT2440 and the EM371 strains were fluorescently tagged with GFP and mCherry. GFP-labeled strains were transformed with Fos expressing plasmids (pSEVA238-AT-Fos), while cherry cells were transformed with Jun (pSEVA238-AT-Jun). (B) Steps followed by the in house designed computational workflow to identify aggregate clusters within confocal microscopy images. Basically, the algorithm follows 4 steps. In step 1, gathered microscopy images were analyzed using Imaris software to obtain geometrical parameters of individual cells such as the mass center position (c), length (L_{bact}), diameter (d_{bact}), and axial orientation vector ($\mathbf{v}_z$). Then, in step 2, distances between cell pairs were computationally arranged into a distance matrix (L^i_j represents the distance between the bacterial centers of no. i to no. j), where each row contains all distance pair combinations of one bacterium (e.g., no. 1) to the rest of the cells indicated (L^1_2, L^1_3 ... L^1_n). After that, in step 3, it was checked that those pair distances (L^i_j) were smaller than or equal to a threshold distance (L^*_{bact}; calculated as the L_{bact} average of all cells of all images) to detect potential contacts. Such a logic evaluation generates a Boolean neighbor matrix where distances satisfying the previous criterium are labeled as "true" and "false" otherwise. Finally, in step 4, every potential contact is confirmed by computing the shortest distance between those cell pairs (d_{PQ}) by using a second proximity criterium ($d_{PQ} \leq d^*_{bact}$, with d^*_{bact} being the average of all cell diameters detected in all images). (C) Representative confocal images of the four types of aggregation experiments performed. In this, GFP and mCherry labeled strains without plasmids (KT2440 and EM371) or with the appropriate pSEVA238-AT-Fos and pSEVA238-AT-Jun plasmids were mixed at a 1:1 ratio and imaged.

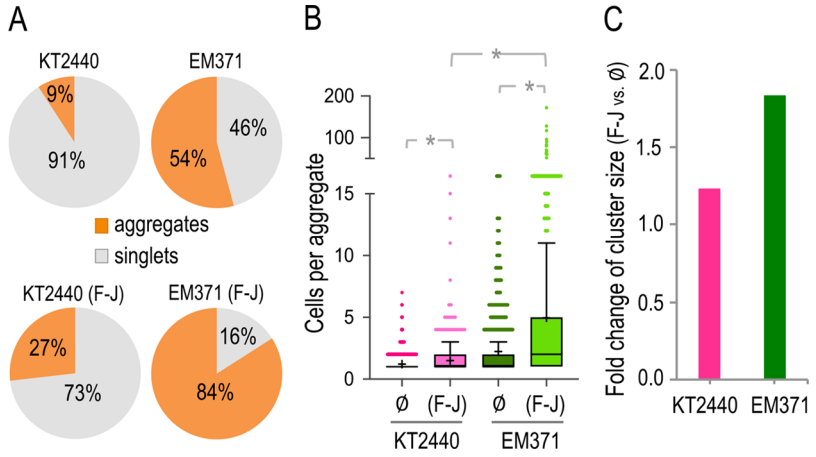

Figure 9. Parameterization of adhesin-mediated *P. putida* cell−cell interplay. (A) Pie charts showing the percentage of cells found as singlets (number of cells ≤ 2) *versus* aggregates ($n > 2$) in the images processed. (B) number of cells per aggregate in each condition represented as a Tukey box-and-whisker plot. The average is represented within a cross, while the median is represented with a horizontal line. Values plotted outside the box represent outliers, meaning that their value is 1.5 times that of the interquartile range (IQR), either below (Q1 − 1.5 × IQR) or above (Q3 + 1.5 × IQR). The asterisk symbol marks significant differences at $P < 0.05$, as assessed by a Mann−Whitney U test. (C) Fold change of cluster size in both strains. This parameter was calculated as the ratio of the average cluster size in the F−J condition to the ones found in the strain without plasmids (ø). The average cluster size was estimated as the fraction of cells identified in aggregates divided by the number of clusters. *P. putida* KT2440 is represented with a pink bar, while EM371 is represented with a green one. For this experiment, two biological replicates and a minimum of 32 images were analyzed.

https://dx.doi.org/10.1021/acssynbio.0c00272
ACS Synth. Biol. 2020, 9, 2477−2492

just biochemical, properties of the bacterial cells. One appealing scenario deals with the ectopic display of enzymatic activities or other functional structures on the cell surface.[99−101] Moreover, rational design of single-strain and multiple-strain consortia with a given composition and 3D architecture is bound to boost the industrial and environmental uses of synthetic biological (SynBio) agents.[2,20,102] Yet, naturally occurring bacteria are most often set evolutionarily with traits at odds with such engineering objectives. In the specific case addressed in this article, the complex organization of the cell surface of *P. putida* not only diverts a good share of metabolic resources for deployment of structures (e.g., EPS, LPS, flagella, fimbriae, *etc.*) that are useless in a reactor (or biotechnological setting thereof) but also limits the spatial accessibility to new functions engineered on the bacterial surface. The results shown above expose the value of stripping the envelope of *P. putida* KT2440 of a number of protruding components to increase exposure of the OM surface to the external medium. The result of this endeavor was *P. putida* EM371, which lost some typical characteristics of strains of this genus but also gained a superior ability to present heterologous proteins anchored on the cell body to the external medium. In this work, this was verified by inspecting surface accessibility of leucine zippers, which barely protrude the OM by a few ångstroms upon display with an autotransporter protein carrier.[103] The utility of the strain to this end has been recently exploited for functional presentation of other, much bigger, structures, *e.g.*, cellulosome scaffoldings.[104] The superior ability of *P. putida* EM371 to ectopically express such proteins is the starting point for a series of strains amenable to *molecular decoration* with increasingly complex structures and/or the ability to act as building blocks of multistrain catalysts.

METHODS

Bacterial Strains, Plasmids, Culture Media, and Growth Conditions. The bacterial strains and plasmids used in this work are shown in Table S4. As rich medium, we used LB (10 g L^{-1} tryptone, 5 g L^{-1} yeast extract, and 5 g L^{-1} NaCl), and for minimal media, we used M9[105] supplemented with different carbon sources at a final concentration of 0.2% (w/v). *P. putida* was incubated at 30 °C, while *E. coli* cells were grown at 37 °C. Antibiotics were used at the following final concentrations: 150 μg mL^{-1} ampicillin (Ap) for *E. coli* and 500 μg mL^{-1} for *P. putida* and 50 μg mL^{-1} kanamycin (Km). To select appropriate clones with the α complementation procedure, we added 40 μg mL^{-1} 5-bromo-4-chloro-3-indolyl-β-D-galactopyranoside (X-gal) plus 1.0 mM isopropyl-β-D-1-thiogalactopyranoside (IPTG) to the LB agar plates. The growth kinetics of both strains with different nutrient conditions was obtained by following the optical density (OD) at 600 nm of the cultures every 15 min, inoculated at an OD_{600} of 0.05, in 96-well microtiter plates using a SpectraMax M2^e microplate reader (Molecular Devices, Sunnyvale, CA, USA). In the case of the final OD_{600} at 24 h, cells of both strains were grown overnight in the appropriate media and then diluted to obtain an initial OD_{600} of 0.005 in 10 mL of the corresponding culture medium and grown at 30 °C with agitation (170 rpm) in 50 mL Erlenmeyer flasks. Then, cultures were vortexed to eliminate clumps, and the OD_{600} values were measured after 24 h of growth.

General DNA Techniques. DNA was manipulated using common laboratory techniques described in ref 105. Plasmid DNA was prepared using the QIAprep Spin Miniprep kit (Qiagen, Inc., Valencia, CA). When required, DNA was purified using the NucleoSpin Extract II (Macherey-Nagel, Düren, Germany). The oligonucleotides used in this work are indicated in Table S2 in the Supporting Information. Colony PCR was performed by transferring cells with a sterile toothpick directly from fresh agar plates into PCR reaction tubes. Suitability of constructs was confirmed by DNA sequencing using primers described in Table S2. Fluorescent derivative strains were obtained by site-specific integration of mini-Tn7 derivatives bearing either constitutively expressed GFP or mCherry fluorescent reporter cassettes.[106,107]

Genome Deletions. Genome deletions were performed using the I-*Sce*I protocol described in refs 34 and 35. Concisely, upstream (TS1) and downstream (TS2) regions of homology were PCR amplified, and both TS1 and TS2 fragments were glued together by means of SOEing PCR.[108] The subsequent TS1−TS2 DNA fragment was digested with appropriate enzymes and cloned into the linearized pEMG plasmid. After that, recombinant plasmids were transformed into *P. putida* cells bearing the pSW-I plasmid,[109] to obtain cointegrates. Once cointegrated clones were obtained, the second recombination event was forced by inducing the expression of the I-*Sce*I endonuclease.[35] Then, Km-sensitive clones were checked by PCR to confirm the corresponding DNA deletion. Finally, after the last genome deletion was done, the pSW-I plasmid was eliminated by growing cells without selective pressure, and the plasmid loss was confirmed first by sensitivity to Ap (500 μg mL^{-1}) and then with colony PCR using oligonucleotides that hybridized with the plasmid backbone (Table S2 in the Supporting Information).

Construction of Plasmids for Surface Display in *P. putida*. Plasmids pJunβ and pFosβ, containing the β-domain of the *igA* protease fused to the transcriptional leucine zippers Jun and Fos were obtained from ref 11. Those constructs were digested with the restriction enzyme NotI and the 1.6 kb fragment cloned into the pSEVA238 expression plasmid.[110,111] The plasmids generated were named pSEVA238-AT-Jun and pSEVA238-AT-Fos (Table S4). The negative control plasmid pSEVA238-trx-$^{G6}V_{HH}$ was constructed as follows: pSEVA238-trx-$^{G6}V_{HH}$ was generated upon digestion of pSEVA-T·G6^{ATG} plasmid[96] with SacI/XbaI, and the 0.8 kb resulting fragment was ligated into the pSEVA238 vector.

Morphological and Phenotypic Assays. For fluorescence microscopy, overnight cultures were diluted in phosphate buffered saline (PBS; 8 mM Na_2HPO_4, 1.5 mM KH_2PO_4, 3 mM KCl, and 137 mM NaCl, pH7) and stained with 5 μg of FM1-43FX for 10 min at room temperature. Next, cells were washed and resuspended in 1 mL of PBS. Then, 3 μL of the membrane stained cells was transferred onto an air-dried coverslip coated with 0.1% (w/v) poly-L-lysine. Finally, DNA was stained with 100 μL of DAPI (4′,6′-diamidino-2-phenylindole; 2 ng μL^{-1}) for 2 min. Images were taken with a confocal multispectral Leica TCS SP5 system (HCX PL Apo CS 100 × 1.4 oil). For quick inspection of bacterial aggregates, overnight grown cultures were diluted to an OD_{600} of 0.1 and grown at 30 °C until OD_{600} 0.5. At that point, cultures were induced with 1 mM 3MBz, and we let them grow for 3 h at 30 °C. After that, samples were mixed at a 1:1 ratio in 10 mL test tubes, and we let them stand for 20 min at room temperature. Then, 5 μL of the bacterial culture was placed onto a slide with 5 μL of Prolong (Life Technologies; Thermo Fisher Scientific) and covered with a 0.1% (w/v) poly-L-lysine coverslip. Samples

https://dx.doi.org/10.1021/acssynbio.0c00272
ACS Synth. Biol. 2020, 9, 2477−2492

were visualized in a Leica DMI600 B fluorescence microscope. To prepare samples for electron microscopy, cells were laid onto carbon-coated collodion grids, negatively stained with 1% (w/v) uranyl acetate, and samples were observed with a JEOL JEOM 1011 transmission electron microscope. To quickly evaluate the lack of motility in the naked strain, 2 μL of overnight cells was spotted onto M9 minimal media with 0.2% (w/v) glucose and solidified with 0.3% (w/v) agar, and plates were incubated at 30 °C for 48 h. Bacterial colony morphology was inspected by spotting 5 μL of overnight grown cultures on M9 minimal media with 0.2% (w/v) glucose or citrate as the carbon source with 40 μg mL^{-1} Congo Red and 20 μg mL^{-1} Coomassie Brilliant Blue. Plates were incubated at 30 °C for 3 days and photographed with a Nikon D60 equipped with an AF-S Micro Nikkor 60 mm f/2.8G ED. For the analysis of the O-antigen, we followed the protocol described in refs 43 and 112. Briefly, cells were grown overnight aerobically at 30 °C, and then, the OD_{600} of cultures was adjusted to 0.4, washed twice with PBS, lysed in SDS−PAGE sample buffer, and treated with proteinase K at 60 °C for 1 h. After that, lipopolysaccharides were separated in a 15% (w/v) SDS−PAGE and visualized by silver staining. We used the MATH score as a proxy to assess surface hydrophobicity.[79,80] For that, exponential cells (OD_{600} ∼ 0.6) were washed with phosphate−urea−magnesium sulfate buffer (97 mM K_2HPO_4, 53.3 mM KH_2PO_4, 30 mM urea, 815 μM $MgSO_4$; pH 7.1). Then, the $OD_{600}^{initial}$ was measured, and 1.2 mL of that cell suspension was mixed with 0.2 mL of hexadecane, vortexed for 45 s, and incubated in a stand for 30 min at RT; the OD_{600}^{final} of the aqueous phase was measured. Thus, the MATH score was calculated as 1-(OD_{600}^{final}/$OD_{600}^{initial}$) × 100. The sedimentation of strains was observed as follows: Cells were grown overnight aerobically at 30 °C in 4 mL of LB. The culture was vortexed, and the OD_{600} was measured and set to 100%; then, tubes were kept at room temperature, standing without agitation, for 24 h, and the OD_{600} of the top part of the culture was estimated. To test the ability of biofilm production, we used the crystal violet assay.[113] Briefly, cells were grown aerobically overnight at 30 °C, and 200 μL of the cells was inoculated into 96-well plates (Thermo Fisher Scientific; MA, USA) at a starting OD_{600} of 0.05 and allowed to grow without agitation at room temperature for 6 h, 24 h, or 4 days. After that, 25 μL of the culture was removed, and the OD_{600} was measured to estimate the density of planktonic cells. Then, plates were washed with water, stained with 0.1% (w/v) crystal violet for 30 min, and washed again with water. Then, the unwashed dye was dissolved with 33% (v/v) acetic acid, and the absorbance at 595 nm was measured (biofilm). Biofilm index represents the ratio of biofilm to OD_{600}. The permeability of the membrane was visually inspected with the CPRG test described.[82] Briefly, cells containing the pSEVA2513-LacZ plasmid that constitutively express the β-galactoside (LacZ) enzyme were streaked on LB agar plates containing 20 μg mL^{-1} of the lactose analogue chlorophenyl red-β-D-galactopyranoside (CPRG), incubated at 30 °C for 24 or 48 h, and photographed. To study the influence of NaCl in the growth physiology, we grew both strains in LB without and with different salt concentrations (from 50 to 400 mM NaCl) at 30 °C with 170 rpm. After overnight growth, we directly measured the OD_{600} of cultures (no vortex), and then, tubes were vortexed for 20 s to disrupt any flock; the OD_{600} was also measured (vortex). Then, the ratio OD_{600}-vortex/OD_{600}-no vortex was calculated and plotted. Bigger numbers for this ratio indicated the presence of bacterial flocks within the liquid media.

Stress Resistance. To evaluate differences in stress resistance between strains, we performed filter disc stressor-soaked experiments in solid media. To do that, we added 100 μL of overnight LB grown cultures to prewarmed 0.7% (w/v) LB top agar, mixed, and overlaid it onto LB agar plates; then, we let it dry. Then, the filter disc was placed in the middle of the agar plate and soaked with 10 μL of the stressor. After that, the plates were incubated at 30 °C for 24 h and photographed, and the diameter of the clear halo generated in both strains was compared.

Protein Extraction, Western Blotting, and Trypsin Digestion. Whole cell protein extracts were prepared collecting cells (OD_{600} ∼ 1.5) by centrifugation, resuspending them in 50 μL of 10 mM Tris−HCl (pH 8.0) and 50 μL of 2x SDS-sample buffer (60 μM Tris−HCl (pH 6.8), 1% (w/v) SDS, 5% (v/v) glycerol, 0.005% (w/v) bromophenol blue, and 1% (v/v) 2-mercaptoethanol), and boiling them for 15 min. Then, samples were sonicated, and cell debris was eliminated by centrifugation for 5 min at 14 000 × g. Supernatants were analyzed on 10% (w/v) SDS−PAGE gels with a Miniprotean III electrophoresis system (Bio-Rad; CA, USA). For Western blots, proteins were transferred to a polyvinylidene difluoride membrane (Immobilon-P; Merck Millipore, MA, USA) using a Trans-Blot SD semidry transfer cell (Bio-Rad; CA, USA) after denaturing electrophoresis. Membranes were first blocked with PBS buffer containing 3% (w/v) skimmed milk for 1 h at room temperature. Then, membranes were incubated for 1 h at room temperature in the same buffer with a 1/2000 dilution of the monoclonal anti-E-tag (Phadia, Sweden) antibody. After that, membranes were washed three times with PBS with 3% (w/v) skimmed milk and 0.1% (v/v) Tween-20 to remove the unbound antibody. Next, a 1/5000 dilution of antimouse IgG conjugated with peroxidase (POD; Merck, MO, USA) was used to reveal the presence of bound anti-E-tag. The light signal was developed by soaking membranes in BM Chemiluminescence Western Blotting Substrate (POD; Merck, MO, USA) for 1 min in the dark and either exposing the membranes to an X-ray film or scanning them in an Amersham Imager 600 (GE Healthcare, IL, USA). Protease accessibility assays were performed as follows: Induced cells were harvested by centrifugation at 4000 × g for 3 min and resuspended in 100 μL of 10 mM Tris−HCl (pH 8.0). Then, this bacterial suspension was incubated with 200 μg mL^{-1} trypsin for 20 min at 37 °C. Subsequently, 5 μg mL^{-1} of trypsin inhibitor was added to stop the proteolysis reaction. Finally, samples were centrifugated at 14 000 × g for 1 min, and the pellet was resuspended in 50 μL of 10 mM Tris−HCl (pH 8.0). Then, whole proteins were extracted and analyzed by Western blot, as described earlier. Bacterial permeabilization was performed by adding 400 μL of lysozyme (20 mg mL^{-1}) to 1 mL of induced cells, which was then incubated for 2 min at RT. Then, cells were washed with 1x PBS and treated with trypsin, as described above, and the presence of the recombinant protein was analyzed by Western blot. Also, permeabilized bacteria were visualized with fluorescence microscopy by incubating cells for 30 min in PBS with 3% (w/v) bovine serum albumin. Then, they were incubated with the anti-E-tag antibody (1:50) at 4 °C. After that, samples were washed three times with PBS and incubated with antimouse IgG Alexa Fluor 594 (1:500; ThermoFisher Scientific) for 30

https://dx.doi.org/10.1021/acssynbio.0c00272
ACS Synth. Biol. 2020, 9, 2477−2492

min in the dark at RT. Finally, cells were visualized in the Leica DMI600 B fluorescence microscope.

Characterization of Surface-Exposed Proteins. To identify surface-exposed proteins, we followed the protocol described in ref 68. Briefly, first nanoparticles were prepared and activated. In order to bind surface-exposed proteins to activated nanoparticles (NPs), *P. putida* cells were grown on LB agar plates overnight, and we scraped them using a sterile loop; then, we washed them with PBS and incubated them for 5 min at 37 °C under stirring in the presence of activated NPs (0.5 mg mL^{-1}). After that, unbound reactive groups on the NPs were blocked with 200 mM Tris−HCl (pH 7.4). Then, cells were disrupted in a French press, and NPs were recovered through a permanent magnet for 1 h at 4 °C; also, they were washed, twice with water and twice with 1 M NaCl, to remove nonspecifically bound material. To remove further non-covalently bound proteins and fragments of the cell envelope, washed NPs from the binding experiments (NP-Env) were incubated for 1 h at 60 °C in the presence of 1% (w/v) SDS. Proteins that remained covalently bound to the SDS-treated NPs (NP-CbP) were then digested with 40 μg mL^{-1} trypsin to break them into fragments suitable for multidimensional protein identification technology (MudPIT) identification.[68] The activity of NPs to capture proteins shed spontaneously from intact cells and proteins released by spontaneous cell lysis was evaluated through control experiments (NP-Shed). In these controls, the cells washed with PBS were incubated for 5 min at 37 °C without NPs and removed by tandem centrifugation−filtration, and the resulting supernatants were incubated for 5 min at 37 °C with activated NPs; in this way, NPs could only react with released proteins. NPs were then inactivated, and the proteins covalently bound to NPs were identified by MudPIT analysis. NP-CbP bound by NPs at the cell surface was listed by statistical comparison[68] of the spectral counts (SpCs) determined by the MudPIT analyses on NP-Env experiments with those of NP-Shed controls. Two independent experiments, both for NP-Env and NP-Shed, were conducted for each strain. The experimental mass spectra produced by MudPIT analyses were correlated to *in silico* peptide sequences of a nonredundant *P. putida* KT2440 protein database retrieved from NCBI (http://www.ncbi.nlm.nih.gov/). Data processing of raw spectra was performed as described in ref 68.

Quantification of Cellular Aggregates. Overnight grown cultures were diluted to an OD_{600} of 0.1, in 100 mL Erlenmeyer flasks containing 10 mL of LB, and grown for 2 h at 30 °C with shaking. Then, cultures were induced overnight by adding 1 mM 3MBz. After that, the aggregation experiments were prepared as follows: Induced cultures were diluted and mixed in a 50 mL flask at a 1:1 ratio to yield a final OD_{600} of 1 in M9 medium without a C-source in a total volume of 4 mL. Then, cells were incubated at RT with moderate orbital shaking (160 rpm) for 30 min. After that, 500 μL samples were taken using head-cut tips to minimize aggregate disruption and combined with 500 μL of melted 2% (w/v) agar M9 without a C-source; then, they were mixed and 250 μL was transferred to a μ-Dish of 35 mm (Ibidi; Germany). Samples were inspected using a confocal multispectral Leica TCS SP8 system with a 100/0.5x oil immersion objective, and images were captured using a 3x amplification factor using a Z-step of 0.5 μm and a refresh frequency of 600 Hz. Virtual 3D reconstruction of aggregates was performed using Imaris software version 10 (BITPLANE; UK) by applying a manual thresholding to the raw image to limit the boundaries of every cell and infering its geometric parameters. Then, the following values were calculated for all detected cells in each fluorescent channel (GFP and mCherry): (i) spatial position ($\mathbf{C}$), (ii) axial orientation ($\mathbf{v}_z$), and (iii) bacterial length (L_{bact}). The values were imported as CSV files. The quantification of aggregates was performed in MATLAB (The Mathworks Inc.; USA) by generating a matrix containing the euclidean distance (L^i_j) among cells. This matrix was used to establish potential cell neighbors. Cells were considered as neighbors if $L^i_j \leq L_{bact}$. All identified potential neighbors were individually inspected with a recurrent depth-first search algorithm using a two spherocylinder contact criterium described in refs 114 and 115 to confirm bacterial contact. Once confirmed as real neighbors, they were tagged as aggregates. The efficiency of aggregation was estimated as (i) the total raw counting of aggregates and (ii) the total fraction of cells within clusters. The analysis was performed with a minimum of 2 biological repetitions, counting at least 500 individual events (cells or aggregates) in total.

■ ASSOCIATED CONTENT

Supporting Information

The Supporting Information is available free of charge at https://pubs.acs.org/doi/10.1021/acssynbio.0c00272.

Genomic coordinates, oligonucleotides used in this study, bacterial strains and plasmids used in this study, genomic regions deleted, growth profiles under different metabolic regimes, permeabilization and trypsin treatment, expression and localization of the Fos and Jun chimera proteins, fluorescent microscopy images of the induced aggregation experiments, and normalized frequency distribution of cells per aggregate (PDF)

List of surface-associated proteins identified by activated magnetic nanoparticles (XLSX)

■ AUTHOR INFORMATION

Corresponding Author

Víctor de Lorenzo − *Systems Biology Program, Centro Nacional de Biotecnología (CNB-CSIC), 28049 Madrid, Spain;* orcid.org/0000-0002-6041-2731; Phone: (34-91) 585 4536; Email: vdlorenzo@cnb.csic.es; Fax: (34-91) 585 4506

Authors

Esteban Martínez-García − *Systems Biology Program, Centro Nacional de Biotecnología (CNB-CSIC), 28049 Madrid, Spain;* orcid.org/0000-0001-8475-7286

Sofía Fraile − *Systems Biology Program, Centro Nacional de Biotecnología (CNB-CSIC), 28049 Madrid, Spain*

David Rodríguez Espeso − *Systems Biology Program, Centro Nacional de Biotecnología (CNB-CSIC), 28049 Madrid, Spain*

Davide Vecchietti − *Department of Biosciences, Università degli Studi di Milano, 20133 Milan, Italy*

Giovanni Bertoni − *Department of Biosciences, Università degli Studi di Milano, 20133 Milan, Italy*

Complete contact information is available at: https://pubs.acs.org/10.1021/acssynbio.0c00272

Author Contributions

E.M.-G., V.d.L., and G.B. planned the experiments; E.M.-G., S.F., D.R.E., and D.V. did the practical work. All authors

https://dx.doi.org/10.1021/acssynbio.0c00272
ACS Synth. Biol. 2020, 9, 2477−2492

analyzed and discussed the data and contributed to the writing of the article.

Funding

This work was funded by the SETH (RTI2018-095584-B-C42) (MINECO/FEDER), SyCoLiM (ERA-COBIOTECH 2018—PCI2019-111859-2) Project of the Spanish Ministry of Science and Innovation. It was also funded by MADONNA (H2020-FET-OPEN-RIA-2017-1-766975), BioRoboost (H2020-NMBP-BIO-CSA-2018-820699), SynBio4Flav (H2020-NMBP-TR-IND/H2020-NMBP-BIO-2018-814650), and MIX-UP (MIX-UP H2020-BIO-CN-2019-870294) Contracts of the European Union and the InGEMICS-CM (S2017/BMD-3691) Project of the Comunidad de Madrid—European Structural and Investment Funds (FSE, FECER).

Notes

The authors declare no competing financial interest.

■ ACKNOWLEDGMENTS

Authors are indebted to Maia Kiviisar (Tartu University, Estonia), Raúl Platero (Instituto Clemente Estable, Uruguay), Cristina Patiño (Electron Microscopy Facility CNB, Madrid), Sylvia Gutiérrez (Advanced Light Microscopy, Madrid), and Pavel Dvorak (Masaryk University, Czech Republic) for valuable advice and help with some experiments.

■ REFERENCES

(1) Hays, S. G., Patrick, W. G., Ziesack, M., Oxman, N., and Silver, P. A. (2015) Better together: engineering and application of microbial symbioses. *Curr. Opin. Biotechnol. 36*, 40−49.

(2) McCarty, N. S., and Ledesma Amaro, R. (2019) Synthetic Biology Tools to Engineer Microbial Communities for Biotechnology. *Trends Biotechnol. 37*, 181−197.

(3) Roell, G. W., Zha, J., Carr, R. R., Koffas, M. A., Fong, S. S., and Tang, Y. J. (2019) Engineering microbial consortia by division of labor. *Microb. Cell Fact. 18*, 35.

(4) Flemming, H.-C., Wingender, J., Szewzyk, U., Steinberg, P., Rice, S. A., and Kjelleberg, S. (2016) Biofilms: an emergent form of bacterial life. *Nat. Rev. Microbiol. 14*, 563−575.

(5) Hall-Stoodley, L., Costerton, J. W., and Stoodley, P. (2004) Bacterial biofilms: from the Natural environment to infectious diseases. *Nat. Rev. Microbiol. 2*, 95−108.

(6) Davey, M. E., and O'toole, G. A. (2000) Microbial Biofilms: from Ecology to Molecular Genetics. *Microbiol. Mol. Biol. Rev. 64*, 847−867.

(7) Jenal, U., Reinders, A., and Lori, C. (2017) Cyclic di-GMP: second messenger extraordinaire. *Nat. Rev. Microbiol. 15*, 271−284.

(8) Römling, U., Galperin, M. Y., and Gomelsky, M. (2013) Cyclic di-GMP: the First 25 Years of a Universal Bacterial Second Messenger. *Microbiol. Mol. Biol. Rev. 77*, 1−52.

(9) Österberg, S., Åberg, A., Herrera Seitz, M. K., Wolf-Watz, M., and Shingler, V. (2013) Genetic dissection of a motility-associated c-di-GMP signalling protein of *Pseudomonas putida*. *Environ. Microbiol. Rep. 5*, 556−565.

(10) Benedetti, I., de Lorenzo, V., and Nikel, P. I. (2016) Genetic programming of catalytic *Pseudomonas putida* biofilms for boosting biodegradation of haloalkanes. *Metab. Eng. 33*, 109−118.

(11) Veiga, E., de Lorenzo, V., and Fernandez, L. A. (2003) Autotransporters as scaffolds for novel bacterial adhesins: surface properties of *Escherichia coli* cells displaying Jun/Fos dimerization domains. *J. Bacteriol. 185*, 5585−5590.

(12) Salema, V., Marín, E., Martínez-Arteaga, R., Ruano-Gallego, D., Fraile, S., Margolles, Y., Teira, X., Gutiérrez, C., Bodelón, G., and Fernández, L. A. (2013) Selection of Single Domain Antibodies from Immune Libraries Displayed on the Surface of *E. coli* Cells with Two *β*-Domains of Opposite Topologies. *PLoS One 8*, e75126.

(13) Piñero-Lambea, C., Bodelón, G., Fernández-Periáñez, R., Cuesta, A. M., Álvarez-Vallina, L., and Fernández, L. A. (2015) Programming Controlled Adhesion of *E. coli* to Target Surfaces, Cells, and Tumors with Synthetic Adhesins. *ACS Synth. Biol. 4*, 463−473.

(14) Glass, D. S., and Riedel-Kruse, I. H. (2018) A Synthetic Bacterial Cell-Cell Adhesion Toolbox for Programming Multicellular Morphologies and Patterns. *Cell 174*, 649−658. e616.

(15) Nikaido, H., and Vaara, M. (1985) Molecular basis of bacterial outer membrane permeability. *Microbiol. Rev. 49*, 1−32.

(16) Nikaido, H. (2003) Molecular Basis of Bacterial Outer Membrane Permeability Revisited. *Microbiol. Mol. Biol. Rev. 67*, 593−656.

(17) Tolker-Nielsen, T. (2015) Biofilm Development. *Microbiol. Spectrum 3*, 1−12.

(18) Martinez-Garcia, E., Nikel, P. I., Aparicio, T., and de Lorenzo, V. (2014) Pseudomonas 2.0: genetic upgrading of *P. putida* KT2440 as an enhanced host for heterologous gene expression. *Microb. Cell Fact. 13*, 159.

(19) Martinez-Garcia, E., and de Lorenzo, V. (2016) The quest for the minimal bacterial genome. *Curr. Opin. Biotechnol. 42*, 216−224.

(20) de Lorenzo, V. (2008) Systems biology approaches to bioremediation. *Curr. Opin. Biotechnol. 19*, 579−589.

(21) Kampers, L. F. C., Volkers, R. J. M., and Martins Dos Santos, V. A. P. (2019) *Pseudomonas putida* KT2440 is HV1 certified, not GRAS. *Microb. Biotechnol. 12*, 845−848.

(22) Jimenez, J. I., Minambres, B., Garcia, J. L., and Diaz, E. (2002) Genomic analysis of the aromatic catabolic pathways from *Pseudomonas putida* KT2440. *Environ. Microbiol. 4*, 824−841.

(23) Kim, J., and Park, W. (2014) Oxidative stress response in *Pseudomonas putida*. *Appl. Microbiol. Biotechnol. 98*, 6933−6946.

(24) Nikel, P. I., Chavarria, M., Danchin, A., and de Lorenzo, V. (2016) From dirt to industrial applications: *Pseudomonas putida* as a Synthetic Biology chassis for hosting harsh biochemical reactions. *Curr. Opin. Chem. Biol. 34*, 20−29.

(25) Ramos, J.-L., Sol Cuenca, M., Molina-Santiago, C., Segura, A., Duque, E., Gómez-García, M. R., Udaondo, Z., and Roca, A. (2015) Mechanisms of solvent resistance mediated by interplay of cellular factors in *Pseudomonas putida*. *FEMS Microbiol. Rev. 39* (4), 555−566.

(26) Martínez-García, E., and de Lorenzo, V. (2017) Molecular tools and emerging strategies for deep genetic/genomic refactoring of *Pseudomonas*. *Curr. Opin. Biotechnol. 47*, 120−132.

(27) Martínez-García, E., Goñi-Moreno, A., Bartley, B., McLaughlin, J., Sánchez-Sampedro, L., Pascual del Pozo, H., Prieto Hernández, C., Marletta, A. S., De Lucrezia, D., Sánchez-Fernández, G., Fraile, S., and de Lorenzo, V. (2020) SEVA 3.0: an update of the Standard European Vector Architecture for enabling portability of genetic constructs among diverse bacterial hosts. *Nucleic Acids Res. 48*, D1164−D1170.

(28) Nikel, P. I., Martinez-Garcia, E., and de Lorenzo, V. (2014) Biotechnological domestication of pseudomonads using synthetic biology. *Nat. Rev. Microbiol. 12*, 368−379.

(29) Poblete-Castro, I., Becker, J., Dohnt, K., dos Santos, V. M., and Wittmann, C. (2012) Industrial biotechnology of *Pseudomonas putida* and related species. *Appl. Microbiol. Biotechnol. 93*, 2279−2290.

(30) Loeschcke, A., and Thies, S. (2015) *Pseudomonas putida*—a versatile host for the production of natural products. *Appl. Microbiol. Biotechnol. 99*, 6197−6214.

(31) Nikel, P. I., and de Lorenzo, V. (2018) *Pseudomonas putida* as a functional chassis for industrial biocatalysis: From native biochemistry to trans-metabolism. *Metab. Eng. 50*, 142−155.

(32) Valls, M., de Lorenzo, V., Gonzàlez-Duarte, R., and Atrian, S. (2000) Engineering outer-membrane proteins in *Pseudomonas putida* for enhanced heavy-metal bioadsorption. *J. Inorg. Biochem. 79*, 219−223.

(33) Winsor, G. L., Lam, D. K., Fleming, L., Lo, R., Whiteside, M. D., Yu, N. Y., Hancock, R. E., and Brinkman, F. S. (2011) *Pseudomonas* Genome Database: improved comparative analysis and population genomics capability for *Pseudomonas* genomes. *Nucleic Acids Res. 39*, D596−600.

https://dx.doi.org/10.1021/acssynbio.0c00272
ACS Synth. Biol. 2020, 9, 2477−2492

(34) Martínez-García, E., and de Lorenzo, V. (2011) Engineering multiple genomic deletions in Gram-negative bacteria: analysis of the multi-resistant antibiotic profile of *Pseudomonas putida* KT2440. *Environ. Microbiol. 13*, 2702−2716.
(35) Martínez-García, E., and de Lorenzo, V. (2012) Transposon-based and plasmid-based genetic tools for editing genomes of Gram-negative bacteria. *Methods Mol. Biol. 813*, 267−283.
(36) Ruer, S., Stender, S., Filloux, A., and de Bentzmann, S. (2007) Assembly of fimbrial structures in *Pseudomonas aeruginosa*: functionality and specificity of chaperone-usher machineries. *J. Bacteriol. 189*, 3547−3555.
(37) Tomaras, A. P., Dorsey, C. W., Edelmann, R. E., and Actis, L. A. (2003) Attachment to and biofilm formation on abiotic surfaces by *Acinetobacter baumannii*: involvement of a novel chaperone-usher pili assembly system. *Microbiology 149*, 3473−3484.
(38) Nuccio, S. P., and Baumler, A. J. (2007) Evolution of the chaperone/usher assembly pathway: fimbrial classification goes Greek. *Microbiol. Mol. Biol. Rev. 71*, 551−575.
(39) Burrows, L. L. (2012) *Pseudomonas aeruginosa* twitching motility: type IV pili in action. *Annu. Rev. Microbiol. 66*, 493−520.
(40) Martínez-García, E., Nikel, P. I., Chavarría, M., and de Lorenzo, V. (2014) The metabolic cost of flagellar motion in *Pseudomonas putida* KT2440. *Environ. Microbiol. 16*, 291−303.
(41) Rocchetta, H. L., Burrows, L. L., and Lam, J. S. (1999) Genetics of O-antigen biosynthesis in *Pseudomonas aeruginosa*. *Microbiol. Mol. Biol. Rev. 63*, 523−553.
(42) Raetz, C. R. H., and Whitfield, C. (2002) Lipopolysaccharide endotoxins. *Annu. Rev. Biochem. 71*, 635−700.
(43) Ramos-Gonzalez, M. I., Ruiz-Cabello, F., Brettar, I., Garrido, F., and Ramos, J. L. (1992) Tracking genetically engineered bacteria: monoclonal antibodies against surface determinants of the soil bacterium *Pseudomonas putida* 2440. *J. Bacteriol. 174*, 2978−2985.
(44) Junker, F., Rodríguez-Herva, J., Duque, E., Ramos-González, M. I., Llamas, M., and Ramos, J. L. (2001) A WbpL mutant of *Pseudomonas putida* DOT-T1E strain, which lacks the O-antigenic side chain of lipopolysaccharides, is tolerant to organic solvent shocks. *Extremophiles 5*, 93−99.
(45) Nelson, K. E., Weinel, C., Paulsen, I. T., Dodson, R. J., Hilbert, H., Martins dos Santos, V. A. P., Fouts, D. E., Gill, S. R., Pop, M., Holmes, M., Brinkac, L., Beanan, M., DeBoy, R. T., Daugherty, S., Kolonay, J., Madupu, R., Nelson, W., White, O., Peterson, J., Khouri, H., Hance, I., Lee, P. C., Holtzapple, E., Scanlan, D., Tran, K., Moazzez, A., Utterback, T., Rizzo, M., Lee, K., Kosack, D., Moestl, D., Wedler, H., Lauber, J., Stjepandic, D., Hoheisel, J., Straetz, M., Heim, S., Kiewitz, C., Eisen, J., Timmis, K. N., Dusterhoft, A., Tummler, B., and Fraser, C. M. (2002) Complete genome sequence and comparative analysis of the metabolically versatile *Pseudomonas putida* KT2440. *Environ. Microbiol. 4*, 799−808.
(46) Espinosa-Urgel, M., Salido, A., and Ramos, J. L. (2000) Genetic analysis of functions involved in adhesion of *Pseudomonas putida* to seeds. *J. Bacteriol. 182*, 2363−2369.
(47) Yousef-Coronado, F., Travieso, M. L., and Espinosa-Urgel, M. (2008) Different, overlapping mechanisms for colonization of abiotic and plant surfaces by *Pseudomonas putida*. *FEMS Microbiol. Lett. 288*, 118−124.
(48) Hinsa, S. M., Espinosa-Urgel, M., Ramos, J. L., and O'Toole, G. A. (2003) Transition from reversible to irreversible attachment during biofilm formation by *Pseudomonas fluorescens* WCS365 requires an ABC transporter and a large secreted protein. *Mol. Microbiol. 49*, 905−918.
(49) Newell, P. D., Monds, R. D., and O'Toole, G. A. (2009) LapD is a bis-(3′,5′)-cyclic dimeric GMP-binding protein that regulates surface attachment by *Pseudomonas fluorescens* Pf0−1. *Proc. Natl. Acad. Sci. U. S. A. 106*, 3461−3466.
(50) Newell, P. D., Boyd, C. D., Sondermann, H., and O'Toole, G. A. (2011) A c-di-GMP effector system controls cell adhesion by inside-out signaling and surface protein cleavage. *PLoS Biol. 9*, e1000587.
(51) Martinez-Gil, M., Yousef-Coronado, F., and Espinosa-Urgel, M. (2010) LapF, the second largest *Pseudomonas putida* protein, contributes to plant root colonization and determines biofilm architecture. *Mol. Microbiol. 77*, 549−561.
(52) Molina, M. A., Ramos, J. L., and Espinosa-Urgel, M. (2006) A two-partner secretion system is involved in seed and root colonization and iron uptake by *Pseudomonas putida* KT2440. *Environ. Microbiol. 8*, 639−647.
(53) Flemming, H.-C., Neu, T. R., and Wozniak, D. J. (2007) The EPS Matrix: The "House of Biofilm Cells. *J. Bacteriol. 189*, 7945−7947.
(54) Nilsson, M., Chiang, W. C., Fazli, M., Gjermansen, M., Givskov, M., and Tolker-Nielsen, T. (2011) Influence of putative exopolysaccharide genes on *Pseudomonas putida* KT2440 biofilm stability. *Environ. Microbiol. 13*, 1357−1369.
(55) Serra, D. O., Richter, A. M., and Hengge, R. (2013) Cellulose as an architectural element in spatially structured *Escherichia coli* biofilms. *J. Bacteriol. 195*, 5540−5554.
(56) Nielsen, L., Li, X., and Halverson, L. J. (2011) Cell-cell and cell-surface interactions mediated by cellulose and a novel exopolysaccharide contribute to *Pseudomonas putida* biofilm formation and fitness under water-limiting conditions. *Environ. Microbiol. 13*, 1342−1356.
(57) Hay, I. D., Wang, Y., Moradali, M. F., Rehman, Z. U., and Rehm, B. H. (2014) Genetics and regulation of bacterial alginate production. *Environ. Microbiol. 16*, 2997−3011.
(58) Chang, W. S., van de Mortel, M., Nielsen, L., Nino de Guzman, G., Li, X., and Halverson, L. J. (2007) Alginate production by *Pseudomonas putida* creates a hydrated microenvironment and contributes to biofilm architecture and stress tolerance under water-limiting conditions. *J. Bacteriol. 189*, 8290−8299.
(59) Svenningsen, N. B., Martinez-Garcia, E., Nicolaisen, M. H., de Lorenzo, V., and Nybroe, O. (2018) The biofilm matrix polysaccharides cellulose and alginate both protect *Pseudomonas putida* mt-2 against reactive oxygen species generated under matric stress and copper exposure. *Microbiology 164*, 883−888.
(60) Larsen, P., Nielsen, J. L., Dueholm, M. S., Wetzel, R., Otzen, D., and Nielsen, P. H. (2007) Amyloid adhesins are abundant in natural biofilms. *Environ. Microbiol. 9*, 3077−3090.
(61) Staley, T. E., Lawrence, E. G., and Drahos, D. J. (1997) Variable specificity of Tn7::*lacZY* insertion into the chromosome of root-colonizing *Pseudomonas putida* strains. *Mol. Ecol. 6*, 85−87.
(62) Choi, K. H., Gaynor, J. B., White, K. G., Lopez, C., Bosio, C. M., Karkhoff-Schweizer, R. R., and Schweizer, H. P. (2005) A Tn7-based broad-range bacterial cloning and expression system. *Nat. Methods 2*, 443−448.
(63) Martinez-Garcia, E., Jatsenko, T., Kivisaar, M., and de Lorenzo, V. (2015) Freeing *Pseudomonas putida* KT2440 of its proviral load strengthens endurance to environmental stresses. *Environ. Microbiol. 17*, 76−90.
(64) Belda, E., van Heck, R. G., José Lopez-Sanchez, M., Cruveiller, S., Barbe, V., Fraser, C., Klenk, H. P., Petersen, J., Morgat, A., Nikel, P. I., Vallenet, D., Rouy, Z., Sekowska, A., Martins Dos Santos, V. A., de Lorenzo, V., Danchin, A., and Médigue, C. (2016) The revisited genome of *Pseudomonas putida* KT2440 enlightens its value as a robust metabolic chassis. *Environ. Microbiol. 18*, 3403−3424.
(65) Olaya-Abril, A., Jimenez-Munguia, I., Gomez-Gascon, L., and Rodriguez-Ortega, M. J. (2014) Surfomics: shaving live organisms for a fast proteomic identification of surface proteins. *J. Proteomics 97*, 164−176.
(66) Giombini, E., Orsini, M., Carrabino, D., and Tramontano, A. (2010) An automatic method for identifying surface proteins in bacteria: SLEP. *BMC Bioinf. 11*, 39.
(67) Doro, F., Liberatori, S., Rodríguez-Ortega, M. J., Rinaudo, C. D., Rosini, R., Mora, M., Scarselli, M., Altindis, E., D'Aurizio, R., Stella, M., Margarit, I., Maione, D., Telford, J. L., Norais, N., and Grandi, G. (2009) Surfome Analysis as a Fast Track to Vaccine Discovery: identification of a novel protective antigen for Group B

https://dx.doi.org/10.1021/acssynbio.0c00272
ACS Synth. Biol. 2020, 9, 2477−2492

Streptococcus hypervirulent strain COH1. *Mol. Cell. Proteomics 8*, 1728−1737.
(68) Vecchietti, D., Di Silvestre, D., Miriani, M., Bonomi, F., Marengo, M., Bragonzi, A., Cova, L., Franceschi, E., Mauri, P., and Bertoni, G. (2012) Analysis of *Pseudomonas aeruginosa* cell envelope proteome by capture of surface-exposed proteins on activated magnetic nanoparticles. *PLoS One 7*, e51062.
(69) Rodriguez-Ortega, M. J., Norais, N., Bensi, G., Liberatori, S., Capo, S., Mora, M., Scarselli, M., Doro, F., Ferrari, G., Garaguso, I., Maggi, T., Neumann, A., Covre, A., Telford, J. L., and Grandi, G. (2006) Characterization and identification of vaccine candidate proteins through analysis of the group A *Streptococcus* surface proteome. *Nat. Biotechnol. 24*, 191−197.
(70) Tjalsma, H., Lambooy, L., Hermans, P. W., and Swinkels, D. W. (2008) Shedding & shaving: disclosure of proteomic expressions on a bacterial face. *Proteomics 8*, 1415−1428.
(71) Tjalsma, H., Scholler-Guinard, M., Lasonder, E., Ruers, T. J., Willems, H. L., and Swinkels, D. W. (2006) Profiling the humoral immune response in colon cancer patients: diagnostic antigens from *Streptococcus bovis*. *Int. J. Cancer 119*, 2127−2135.
(72) Tjalsma, H., Lasonder, E., Schöller-Guinard, M., and Swinkels, D. W. (2007) Shotgun immunoproteomics to identify disease-associated bacterial antigens: Application to human colon cancer. *Proteomics: Clin. Appl. 1*, 429−434.
(73) Harshey, R. M. (2003) Bacterial motility on a surface: many ways to a common goal. *Annu. Rev. Microbiol. 57*, 249−273.
(74) Espeso, D. R., Martínez-García, E., de Lorenzo, V., and Goñi-Moreno, A. (2016) Physical forces shape group identity of swimming *Pseudomonas putida* cells. *Front. Microbiol. 7*, 1437.
(75) Romling, U., Bian, Z., Hammar, M., Sierralta, W. D., and Normark, S. (1998) Curli fibers are highly conserved between *Salmonella typhimurium* and *Escherichia coli* with respect to operon structure and regulation. *J. Bacteriol. 180*, 722−731.
(76) Friedman, L., and Kolter, R. (2004) Genes involved in matrix formation in *Pseudomonas aeruginosa* PA14 biofilms. *Mol. Microbiol. 51*, 675−690.
(77) Pesavento, C., Becker, G., Sommerfeldt, N., Possling, A., Tschowri, N., Mehlis, A., and Hengge, R. (2008) Inverse regulatory coordination of motility and curli-mediated adhesion in *Escherichia coli*. *Genes Dev. 22*, 2434−2446.
(78) Serra, D. O., Richter, A. M., Klauck, G., Mika, F., and Hengge, R. (2013) Microanatomy at cellular resolution and spatial order of physiological differentiation in a Bacterial Biofilm. *mBio 4*, e00103−13.
(79) Rosenberg, M., Gutnick, D., and Rosenberg, E. (1980) Adherence of bacteria to hydrocarbons: A simple method for measuring cell-surface hydrophobicity. *FEMS Microbiol. Lett. 9*, 29−33.
(80) Rosenberg, M. (1984) Bacterial adherence to hydrocarbons: a useful technique for studying cell surface hydrophobicity. *FEMS Microbiol. Lett. 22*, 289−295.
(81) Lahesaare, A., Ainelo, H., Teppo, A., Kivisaar, M., Heipieper, H. J., and Teras, R. (2016) LapF and Its Regulation by Fis Affect the Cell Surface Hydrophobicity of *Pseudomonas putida*. *PLoS One 11*, e0166078.
(82) Paradis-Bleau, C., Kritikos, G., Orlova, K., Typas, A., and Bernhardt, T. G. (2014) A genome-wide screen for bacterial envelope biogenesis mutants identifies a novel factor involved in cell wall precursor metabolism. *PLoS Genet. 10*, e1004056.
(83) Delcour, A. H. (2009) Outer membrane permeability and antibiotic resistance. *Biochim. Biophys. Acta, Proteins Proteomics 1794*, 808−816.
(84) Nikel, P. I., Fuhrer, T., Chavarria, M., Sanchez-Pascuala, A., Sauer, U., and de Lorenzo, V. (2020) Redox stress reshapes carbon fluxes of *Pseudomonas putida* for cytosolic glucose oxidation and NADPH generation. *bioRxiv*, 1.
(85) Rubin, A. J., Hayden, P. L., and Hanna, G. P. (1969) Coagulation of *Escherichia coli* by neutral salts. *Water Res. 3*, 843−852.
(86) Lindahl, M., Faris, A., Wadstrom, T., and Hjerten, S. (1981) A new test based on 'salting out' to measure relative surface hydrophobicity of bacterial cells. *Biochim. Biophys. Acta, Gen. Subj. 677*, 471−476.
(87) Arakawa, T., and Timasheff, S. N. (1984) Mechanism of protein salting in and salting out by divalent cation salts: balance between hydration and salt binding. *Biochemistry 23*, 5912−5923.
(88) Israelachvili, J., and Wennerstrom, H. (1996) Role of hydration and water structure in biological and colloidal interactions. *Nature 379*, 219−225.
(89) Marrink, S. J., Berkowitz, M., and Berendsen, H. J. C. (1993) Molecular dynamics simulation of a membrane/water interface: the ordering of water and its relation to the hydration force. *Langmuir 9*, 3122−3131.
(90) Watanabe, N., Suga, K., and Umakoshi, H. (2019) Functional Hydration Behavior: Interrelation between Hydration and Molecular Properties at Lipid Membrane Interfaces. *J. Chem. 2019*, 4867327.
(91) O'Toole, G. A., and Kolter, R. (1998) Flagellar and twitching motility are necessary for *Pseudomonas aeruginosa* biofilm development. *Mol. Microbiol. 30*, 295−304.
(92) Pratt, L. A., and Kolter, R. (1998) Genetic analysis of *Escherichia coli* biofilm formation: roles of flagella, motility, chemotaxis and type I pili. *Mol. Microbiol. 30*, 285−293.
(93) Sauer, K., Cullen, M. C., Rickard, A. H., Zeef, L. A. H., Davies, D. G., and Gilbert, P. (2004) Characterization of nutrient-induced dispersion in *Pseudomonas aeruginosa* PAO1 biofilm. *J. Bacteriol. 186*, 7312−7326.
(94) Tolker-Nielsen, T., Brinch, U. C., Ragas, P. C., Andersen, J. B., Jacobsen, C. S., and Molin, S. (2000) Development and Dynamics of *Pseudomonas* sp. Biofilms. *J. Bacteriol. 182*, 6482−6489.
(95) Abate, C., Luk, D., Gentz, R., Rauscher, F. J., and Curran, T. (1990) Expression and purification of the leucine zipper and DNA-binding domains of Fos and Jun: both Fos and Jun contact DNA directly. *Proc. Natl. Acad. Sci. U. S. A. 87*, 1032−1036.
(96) Jimenez, J. I., Fraile, S., Zafra, O., and de Lorenzo, V. (2015) Phenotypic knockouts of selected metabolic pathways by targeting enzymes with camel-derived nanobodies (V(HH)s. *Metab. Eng. 30*, 40−48.
(97) Klauser, T., Pohlner, J., and Meyer, T. F. (1990) Extracellular transport of cholera toxin B subunit using *Neisseria* IgA protease beta-domain: conformation-dependent outer membrane translocation. *EMBO J. 9*, 1991−1999.
(98) Besingi, R. N., and Clark, P. L. (2015) Extracellular protease digestion to evaluate membrane protein cell surface localization. *Nat. Protoc. 10*, 2074−2080.
(99) Salema, V., and Fernandez, L. A. (2017) *Escherichia coli* surface display for the selection of nanobodies. *Microb. Biotechnol. 10*, 1468−1484.
(100) Schuurmann, J., Quehl, P., Festel, G., and Jose, J. (2014) Bacterial whole-cell biocatalysts by surface display of enzymes: toward industrial application. *Appl. Microbiol. Biotechnol. 98*, 8031−8046.
(101) Wernerus, H., and Stahl, S. (2004) Biotechnological applications for surface-engineered bacteria. *Biotechnol. Appl. Biochem. 40*, 209−228.
(102) Gilbert, C., and Ellis, T. (2019) Biological Engineered Living Materials: Growing Functional Materials with Genetically Programmable Properties. *ACS Synth. Biol. 8*, 1−15.
(103) Heras, B., Totsika, M., Peters, K. M., Paxman, J. J., Gee, C. L., Jarrott, R. J., Perugini, M. A., Whitten, A. E., and Schembri, M. A. (2014) The antigen 43 structure reveals a molecular Velcro-like mechanism of autotransporter-mediated bacterial clumping. *Proc. Natl. Acad. Sci. U. S. A. 111*, 457−462.
(104) Dvorak, P., Bayer, E., and de Lorenzo, V. (2020) Surface display of designer protein scaffolds on genome-reduced strains of *Pseudomonas putida*. *bioRxiv*, 1.
(105) Sambrook, J., Maniatis, T., and Fritsch, E. F. (1989) *Molecular Cloning a Laboratory Manual*, Cold Spring Harbor Laboratory Press, Cold Spring Harbor, New York.

https://dx.doi.org/10.1021/acssynbio.0c00272
ACS Synth. Biol. 2020, 9, 2477−2492

(106) Koch, B., Jensen, L. E., and Nybroe, O. (2001) A panel of Tn7-based vectors for insertion of the *gfp* marker gene or for delivery of cloned DNA into Gram-negative bacteria at a neutral chromosomal site. *J. Microbiol. Methods 45*, 187−195.
(107) Rochat, L., Pechy-Tarr, M., Baehler, E., Maurhofer, M., and Keel, C. (2010) Combination of fluorescent reporters for simultaneous monitoring of root colonization and antifungal gene expression by a biocontrol pseudomonad on cereals with flow cytometry. *Mol. Plant-Microbe Interact. 23*, 949−961.
(108) Horton, R. M., Hunt, H. D., Ho, S. N., Pullen, J. K., and Pease, L. R. (1989) Engineering hybrid genes without the use of restriction enzymes: gene splicing by overlap extension. *Gene 77*, 61−68.
(109) Wong, S. M., and Mekalanos, J. J. (2000) Genetic footprinting with mariner-based transposition in *Pseudomonas aeruginosa*. *Proc. Natl. Acad. Sci. U. S. A. 97*, 10191−10196.
(110) Silva-Rocha, R., Martínez-García, E., Calles, B., Chavarría, M., Arce-Rodríguez, A., de Las Heras, A., Páez-Espino, A. D., Durante-Rodríguez, G., Kim, J., Nikel, P. I., Platero, R., and de Lorenzo, V. (2013) The Standard European Vector Architecture (SEVA): a coherent platform for the analysis and deployment of complex prokaryotic phenotypes. *Nucleic Acids Res. 41*, D666−675.
(111) Martinez-Garcia, E., Aparicio, T., Goni-Moreno, A., Fraile, S., and de Lorenzo, V. (2015) SEVA 2.0: an update of the Standard European Vector Architecture for de-/re-construction of bacterial functionalities. *Nucleic Acids Res. 43*, D1183−1189.
(112) Hitchcock, P. J., and Brown, T. M. (1983) Morphological heterogeneity among Salmonella lipopolysaccharide chemotypes in silver-stained polyacrylamide gels. *J. Bacteriol. 154*, 269−277.
(113) O'Toole, G. A. (2011) Microtiter dish biofilm formation assay. *J. Visualized Exp. 47*, 2437.
(114) Vega, C., and Lago, S. (1994) A fast algorithm to evaluate the shortest distance between rods. *Comput. Chem. 18*, 55−59.
(115) Pournin, L., Weber, M., Tsukahara, M., Ferrez, J.-A., Ramaioli, M., and Liebling, T. M. (2005) Three-dimensional distinct element simulation of spherocylinder crystallization. *Granular Matter 7*, 119−126.

https://dx.doi.org/10.1021/acssynbio.0c00272
ACS Synth. Biol. 2020, 9, 2477−2492